THESIS FOR THE DEGREE OF DOCTOR OF PHILOSOPHY

Coagulation of Cellulose: from Ionic-Liquid Solution to Cellulose Nanostructure

Artur Hedlund

Department of Chemistry and Chemical Engineering
CHALMERS UNIVERSITY OF TECHNOLOGY
Gothenburg, Sweden 2018

Coagulation of Cellulose: from Ionic-Liquid Solution to Nanostructure

ARTUR HEDLUND
ISBN 978-91-978-91-7597-757-7

Doktorsavhandlingar vid Chalmers tekniska högskola.
Ny serie Nr 4438
ISSN 0346-718X

Department of Chemistry and Chemical Engineering
Chalmers University of Technology
SE-412 96 Gothenburg
Sweden
Telephone + 46 (0)31-772 1000

Cover:
Aquarelief, Pars pro toto, in polyamide, by Lars Englund in 1973

Chalmers Reproservice
Gothenburg, Sweden 2018

Coagulation of Cellulose: From Ionic-Liquid Solution to Cellulose Nanostructure

Artur Hedlund

Forest Products and Chemical Engineering
Department of Chemistry and Chemical Engineering
CHALMERS UNIVERSITY OF TECHNOLOGY

Abstract

A linear chain of glucose monomers, cellulose, provides the structural reinforcement of the cell walls of plants and constitutes almost half of their dry mass. Wood and other plant-based raw materials are processed on a large industrial scale to isolate the cellulose, which is then dissolved. The resulting solutions can be shaped into films or fibers and solidified as such by immersion in a nonsolvent. The properties of the solidified cellulose products can, however, vary and are frequently not quite satisfactory. In the solidification process, cellulose forms one phase and the nonsolvent and solvent form a second phase, which is later removed through washing and drying. However, these phase separations of ternary mixtures are more complicated than the sentence above indicates. In fact, the details left out decide the properties of those variable materials.

This thesis reports on the interdependencies between several parameters and aspects that are critical to cellulose phase separations: compound properties, phase equilibria for the ternary mixtures, the diffusion processes, and the nanostructures formed. Several new experimental methods were developed to measure the critical amounts of nonsolvent that induce coagulation, the mass transport of solvent and nonsolvent, and the rates of coagulation. The cellulose solutions of an ionic liquid, 1ethyl-3methyl-imidazolium acetate, [C_2mim][OAc], with varied amounts of a cosolvent, DMSO, were coagulated in water, ethanol (EtOH), or 2-propanol (2PrOH). It was found that 2PrOH is, expressed in molar ratio, the strongest nonsolvent (> EtOH > water). However, the diffusive rates, *D*, and coagulation rates were in the opposite order (water > EtOH > 2PrOH). The observed differences between nonsolvent compounds were much larger for $D_{[C2mim][OAc]}$ than for $D_{NonSolvent}$, for the rates of coagulation or for D_{DMSO}, particularly with high cellulose concentration.

More differences between water and alcohol as the nonsolvent were observed in the cellulose structures formed. Coagulation in water produced relatively well-ordered crystalline structures, whereas coagulation in alcohol did not. The differences between water and alcohol as the nonsolvent can be explained by different modes of phase separation and differences in nonsolvent interactions with [C_2mim][OAc] and cellulose. To show the reader how we arrived at those conclusions, which have not been found in previous literature in the cellulose field, a substantial background regarding the properties and interactions of the compounds is supplied.

Networks of cellulose nanofibrils were formed in all the nonsolvents tested, which explained the generally high diffusivities observed and the minor effect of cellulose on diffusion. It appeared that diffusion through the cellulose nanofibril network is similar to diffusion in a mixture of [C_2mim][OAc] and nonsolvent only, which was confirmed with a simplistic computer model.

Keywords: Cellulose, Ionic Liquids, Nonsolvent, Coagulation, Diffusion, Wet Spinning

List of publications

This thesis is based on the work contained in the following papers, referred to by roman numerals in the text. The articles are appended at the end of the thesis.

I. **Coagulation of EmimAc-cellulose solutions: dissolution-precipitation disparity and effects of non-solvents and cosolvent.**
A. Hedlund, T. Köhnke, and H. Theliander
NORDIC PULP & PAPER RESEARCH JOURNAL, 2015. **30**(1): p. 32-42.

II. **Diffusion in Ionic Liquid-Cellulose Solutions during Coagulation in Water: Mass Transport and Coagulation Rate Measurements.**
A. Hedlund, T. Köhnke, and H. Theliander
Macromolecules, 2017. **50**(21): p. 8707-8719.

III. **Microstructures of cellulose coagulated in water and alcohols from 1-ethyl-3-methylimidazolium acetate: Contrasting coagulation mechanisms**
A. Hedlund, J. Hagman, T. Köhnke, U. Olsson, and H. Theliander
(Submitted to Cellulose)

IV. **Mass Transport during Coagulation of Cellulose-Ionic Liquid Solutions in Different Non-Solvents**
A. Hedlund, T. Köhnke, and H. Theliander
(Manuscript ready for submission)

Contribution report

The authors contribution to the papers in this thesis:

I. Main author. Development of experimental method, development and construction of equipment with which to perform the measurements, planning and execution of the measurements, evaluation and interpretation of results and writing.

II. Main author. Development of experimental method, development and construction of equipment with which to perform the measurements, planning and execution of the measurements, evaluation and interpretation of results, construction of numeric model and writing. DMSO analysis with NMR was done elsewhere.

III. Main author. Planning, sample preparation, BET measurements, evaluation and interpretation of results and writing. The XRD measurements were performed with the help of Joel Hagman at Lund University. The SEM images were taken by Melina da Silva, at Swerea IVF.

IV. Main author. Planning and execution of the measurements, evaluation and interpretation of results and writing. DMSO analysis with NMR was done elsewhere.

Although the author has written the articles, the supervisors have been frequent with feedback, advice and detailed suggestions for improvements, not least regarding the outline of Papers II and IV.

Conference presentations

The progress of this work has been presented at several conferences and meetings:

i. **Coagulation Values of Cellulose-Ionic Liquid-DMSO solutions**
NAROTEC September, 2014, Erfurt, Germany

ii. **Investigations into the coagulation of cellulose from EmimAc-DMSO solutions in common protic solvents**
COST FP1205 Training School Pretreatment and dissolution of cellulose, April 07-09, 2015, Jena, Germany

iii. **Coagulation and structure formation of cellulose from EmimAc-DMSO solutions.**
5th Avancell conference, October 6-7 2015, Göteborg, Sweden

iv. **Structure of cellulose materials coagulated from different EmimAc-DMSO solutions** Proceedings of COST Action FP1205, Warsaw, October, 18, pp 42-43. (poster)

v. **Measurements of mass transport during coagulation of cellulose-EmimAc-DMSO solutions.**
4th EPNOE international Polysacharide Conference, Warsaw, Poland, October 19-22 2015, p. 163.

vi. **Structure of cellulose coagulated from different EmimAc-DMSO solutions**
Proceedings of COST Action FP1205, Borås, Sweden, April 13-14, 2016.

vii. **Coagulation of cellulose-ionic liquid solutions for textile fiber production**
Proceedings of the 2016 MWP Event Global Wood Science Days for Young Scientists, Stockholm, Sweden, October 10-13, 2016.

viii. **Coagulation of cellulose solutions and controlling properties of regenerated cellulose materials**
Proceedings of the Final meeting in COST FP1205, Cellulosic material Properties and industrial potential, Stockholm, Sweden, March 7-9, 2017

Additional publications

Apart from the included papers, the author has also made minor contributions to the following articles:

i. **Effect of methylimidazole on cellulose/ionic liquid solutions and regenerated material therefrom.**
C. Olsson, A. Hedlund, A. Idström and G. Westman
Journal of Materials Science, 2014. 49(9): p. 3423-3433.

ii. **Understanding the Inhibiting Effect of Small-Molecule Hydrogen Bond Donors on the Solubility of Cellulose in Tetrabutylammonium Acetate/DMSO**
J. Bengtsson, C. Olsson, A. Hedlund, T. Köhnke and E. Bialik
The Journal of Physical Chemistry B, 2017. 121(50): p. 11241-11248.

Contents

1 Introduction

In 2013, we set out to understand "how" and "why" cellulose, the perhaps simplest polysaccharide on earth, can form such different structures when dissolved and then precipitated. We planned many investigations and initiated some studies. This thesis contains findings from the studies that have been completed.

1.1 Background

The dissolution of cellulose was achieved at the end of the 19th century, before it was confirmed to be a linear chain of covalently bonded monomers. It was soon realized that the solutions could be precipitated in various shapes like fibers and films. Synthetic "silk," cellophane, and sausage casings could be produced on industrial scale. In such wet-spinning processes (of fibers), cellulose solutions are extruded through capillaries ~0.1 mm thick and emerge as solution jets in the coagulation liquid and become more or less solid. The viscose process, in which cellulose is derivatized with hazardous CS_2, dissolved in NaOH, and then precipitated in sulfuric acid, soon became the dominant process. At the time, the health of workers and pollution were not important concerns. Today, there is no production in the Nordic countries and only a few plants remain in Europe. Competition from new petroleum-based fibers and a need for new investments to modernize existing plants were probably the main reasons for the industry's decline during the second half of the 20th century. The growth in volume during the last decade has been limited to Asia (with the exception of Lenzing in Austria). However, the volume of raw material, dissolving pulp, produced in Sweden would be sufficient for a full scale viscose plant. The main obstacles to the re-establishment of viscose plants in Sweden are environmental regulations and costs for adhering to those regulations. Additional issues are the consumption of CS_2 and the continuous bi-production of Na_2SO_4 from the neutralization of NaOH with H_2SO_4, which is about as large as the production of fiber.

However, alternative processes based on extremely polar hydrogen bond accepting (HBA) solvents exist that do not require the derivatization of cellulose to dissolve it. For example, N-

methyl-morpholine-N-oxide (NMMO) monohydrate is used to produce about 200kt/a of lyocell fibers, globally. This is a moderate increase since the first plant of 50kt/a was started in 1990 [1]. [2]

More recent examples of HBA cellulose solvents are the ionic liquids (ILs)[3, 4], which constitute a large group of solvents that remain to be commercialized industrially. All of these HBA-solvent cellulose solutions can be precipitated in water and alcohols that can be evaporated to recover the solvent, which has negligible vapor pressure. Thus, these new solvents offer the prospect of full chemical recycling, which is necessary given their higher prices.

One advantage of the viscose process is its versatility. Whereas lyocell fibers are strong and stiff, it has been difficult to tailor their properties to suit different applications. One potential advantage of the ionic liquids over NMMO and particularly over viscose could be the moderate complexity of processing, which would allow their implementation for niche products. However, for such niche products to come about, scientists and engineers must learn how to change the material structures and properties of regenerated cellulose from default ones to extraordinary ones.

This thesis aims to clarify how parameters, like nonsolvent characteristics, cellulose concentrations and the addition of cosolvent, affect the coagulation of cellulose-IL solution strands, which is induced when the strands contact the nonsolvent. What happens, in detail on the nanoscale, when the cellulose solidifies and the IL solvent is washed out by the nonsolvent? To the human eye, the coagulation appears instantaneous, as it typically takes place inside a fiber that is less than 0.1 mm thick and moving at ~1 m/s during fiber spinning. To examine the kinds of materials formed and how the final material structures were affected by the process parameters, we had to find new methods to isolate parts of the process and investigate these parts under more controlled conditions. We studied how compound properties, chemical conditions, and physical processes are interdependent. These interdependencies are general for cellulose-IL dissolution and precipitation in protic nonsolvent. As our method, we chose to work with one already frequently studied IL, [C_2mim][OAc], a cosolvent, DMSO, and three nonsolvents (water, ethanol, and 2-propanol). Understanding the fundamental aspects of one IL is worth more than bits and pieces of data from different ILs.

1.2 Thesis Outline

Subsections 2.1-2.4 present a selection of previous knowledge on relevant physical and chemical phenomena and on relevant aspects of some compounds that are central to the thesis. The focus is on enthalpic aspects and interaction energies, as these are of particular importance to cellulose dissolution and precipitation in ILs and, therefore, provide the best explanations for the various results observed. Section 3 briefly presents methods. Detailed information about the methods developed during the study can be found in the published papers. Each subsection of Results (4) begins with a background containing pertinent previous knowledge on that particular subject. Subsection 4.1 summarizes the investigations of the phase diagrams for precipitation in water, EtOH, and 2PrOH, as reported in Paper I.

Subsection 4.2 is a synthesis of the results of Papers II and IV on mass transport during immersion precipitation of solutions in the same nonsolvents as in Subsection 4.1. Subsection 4.2 also brings up several theoretical aspects of the transient mass transport during coagulation that, although these aspects are deducible from previous knowledge, have not been frequently discussed or not always correctly treated in previous reports. In Subsection 4.3, the structures of the material formed in 4.2 are presented and discussed. Each subsection ends with a list of conclusions. Not all of these are included in Conclusion (5), which contains only the central observations made.

2 Previous Knowledge

2.1 Phase Separation

Many materials that we encounter in everyday life change phase by melting, freezing, or evaporating. One homogeneous phase changes into another. For instance, eggs solidify upon heating, paint dries, and salt dissolves in water. In these cases, the number of phases is not equal before and after the phase transition. One phase can separate into two, or two phases can mix to become one. Such are the processes for cellulose mixed in solvent treated in this thesis.

2.1.1 Solubility

The thermodynamic stability of a homogeneous mixture (solution) of multiple compounds is decided by the Gibbs free energy of solution, defined in Eq. 1, in which $\Delta[\,]_{sol}$ represents the difference between the mixture and the sum of the separate compounds ($[\,]_{AB} - ([\,]_A + [\,]_B$)).

$$\Delta G_{sol} = \Delta H_{sol} - T\Delta S_{sol} \quad (1)$$

The entropic contribution, $-T\Delta S_{sol}$, favors the dissolved state due to translational freedom for all compounds throughout the whole volume, whereas the enthalpic part, ΔH_{sol}, can be either positive or negative depending on the specific interactions between the compounds, as exemplified in Fig. 1. A condition for producing a solution is that $\Delta G_{sol} < 0$, and likewise the primary requirement for the opposite process is that the sign of ΔG_{sol} is inversed (> 0), which can happen as a result of reducing the temperature or changing the concentration. The latter is the subject of this thesis: the introduction of a nonsolvent that can change the *H* and *S* of both the mixture and the separate phases. This thesis is limited to polymer solutions, of which free energy curves are asymmetric because the polymer contributes very little to the entropic part. Because the M_w of the polymer is much larger than the M_w of the solvent, most of ΔS_{sol} is due to that the more numerous solvent molecules gain access to the volume that was occupied by polymer prior to dissolution. This volume is relatively small, which limits the importance

of the entropic contribution to ΔG_{sol}. In contrast, ΔS_{mix} is more important for the infusion of nonsolvents, of which M_w is much smaller. [5]

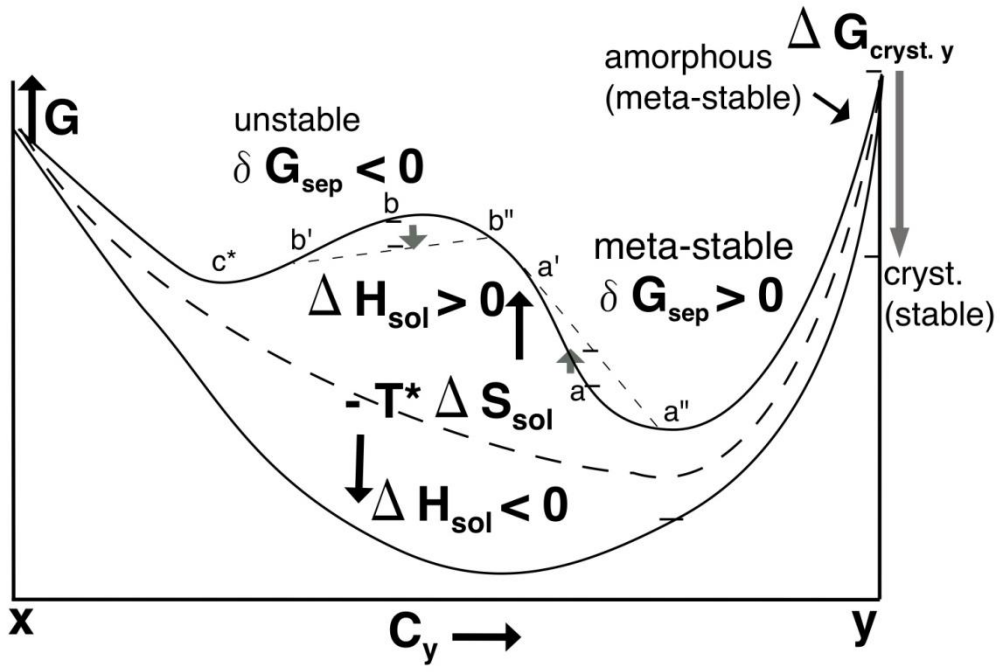

Figure 1. Schematic examples of free energy (*G*) curves for the mixtures of components *x* (concentrated to the left) and *y* (polymer, concentrated to the right). The hatched curve is the entropic part (*-TΔS*) and the solid curves include the enthalpic part (*ΔH*). Compositions *a* and *b* serve to exemplify meta-stability. Both would minimize their *G* by separating into *c** and *a"*, but only *b* can reduce *G* by the initial separation into *b*' and *b"*, whereas *a* is restrained by an initial increase in *G*. $\Delta G_{cryst.}$ is the heat that can be released if *y* is allowed to crystallize.

2.1.2 Meta-Stability

The stability of an existing single phase (a solution) can be maintained even with $\Delta G_{sol} > 0$, if the initial separation into slightly different concentrations for the two new phases corresponds to a higher total *G* than the homogeneous mixture. This situation is exemplified at point *a* in Fig. 1, where an incremental separation leads to an increase in total *G* . This is indicated by the tie-line between the new separated compositions *a'* and *a"* ,which is above *a*. At points *b*, *b'*,and *b"* , the sign of *δG* is the opposite (*<0*), which makes the composition at *b* unstable and the separation spontaneous. Meta-stability is clearly decided by the concavity or convexity of the curve. Such barriers to separation can also result from the surface tension between the newly formed phases. The surface energy per volume is $\sim 1/r$, which becomes very large for objects of small radius, *r*, and makes the small domains of a separated phase unstable and less prone to form. Similarly, small crystals have a higher *G* and are less stable than large crystals. Therefore, dynamic parameters can actually change *G* and ΔG_{sol} (the thermodynamic equilibrium) by enabling varying degrees of order in the pure polymer phase (see right *G*-axis in Fig.1). [6]

2.1.3 Modes of Phase Separation

The existence of free energy barriers and meta-stable states and the mechanisms that release their latent free energy are central parameters of phase separation. These parameters are often decisive for the kind of structures that are formed. If phase separation starts spontaneously as in *b* (Fig. 1), then both b' and b" form in parallel.

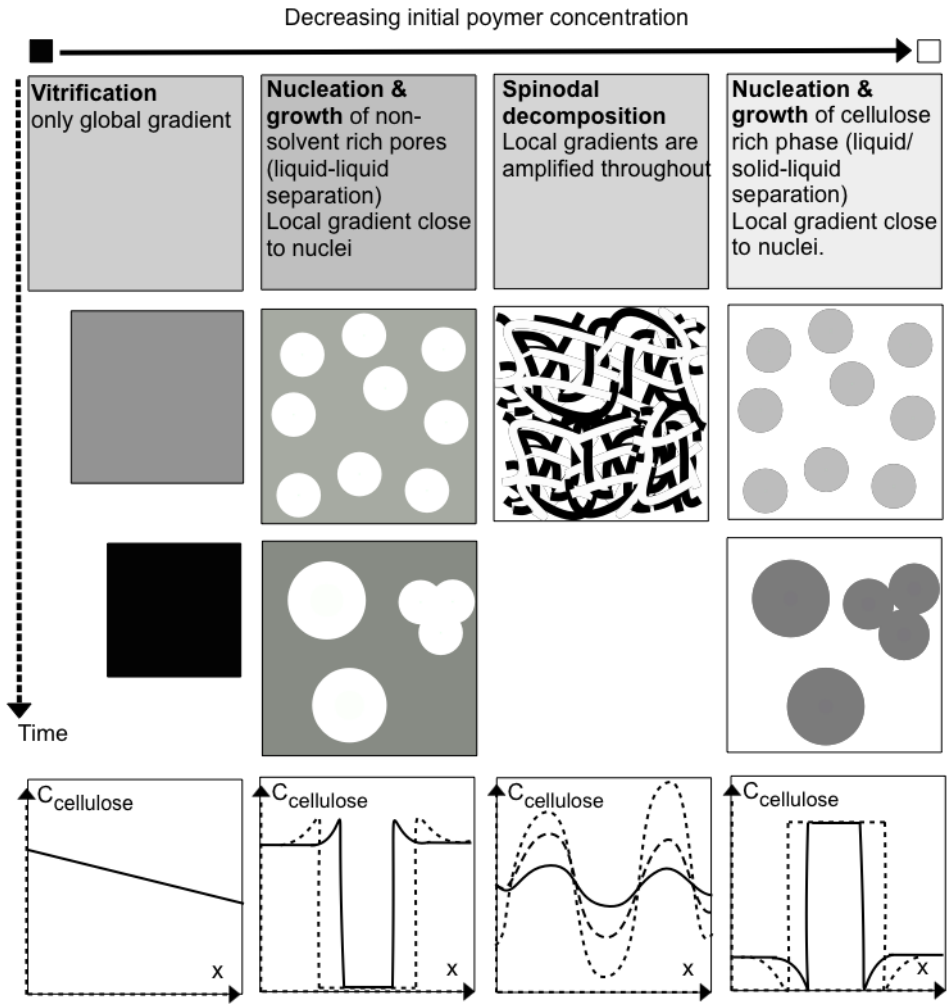

Figure 2. Overview of the different known types of phase separation, ordered column wise according to declining polymer concentration, left to right (a general tendency), and ordered vertically (progression in time). Increasing polymer concentration is indicated with darker shades, and non-solvent domains are white. The characteristic concentration gradients for each type are provided below each column, and the gradual development in time is illustrated with hatched lines.

This mode of separation is termed spinodal and generally results in fine bi-continuous structures. It is more probable at "intermediate" concentrations. However, what is "intermediate" depends on the system at hand. Most phase separation experiments have focused on thermally induced phase separations in bi-component systems, whereas ternary systems contain additional factors such as how components are divided between phases. At concentrations below or above "intermediate," one phase forms minor separate individual domains that gradually increase in size. This mode of separation is termed nucleation and

growth. The formation of minor-phase nuclei typically follows some degree of super-saturation at meta-stable compositions (*a* in Fig.1). The resulting structures can contain either liquid pores or nodular particles as the result of the minor domains, depending on which phase is nucleating. A third separation mode, vitrification, generally occurs when the solvent evaporates, or when an increase in polymer concentration is incurred in any way, without a well-defined phase separation. This is generally not possible in cellulose solutions, however, it could be arranged, at least in theory. For example, a very weak relatively hydrophobic coagulant, such as a large alcohol or ketone, that is not soluble in the solution, but in which the IL still has some minor solubility, could allow the IL to leave without incurring a clear phase separation. However, the time required for this to happen would be very long. Figure 2 summarizes some key features of these three modes. [7]

2.1.4 Solid-Liquid Separations

In most polymer solutions, the primary separation gives two liquid phases: one rich in polymer and a second rich in nonsolvent. However, if the polymer can crystallize and release considerable enthalpy in the process, crystallization into a solid phase can be favored over the entropically favored liquid alternative. In such cases, solid-liquid separation can replace liquid-liquid separation, given sufficient time for crystallization to take place[7]. The propensity for solid-liquid relative to liquid-liquid separation has been estimated [8] based on the theories of Flory-Huggins. In that study, the findings were that low nonsolvent affinities for polymer and solvent favor liquid-liquid separation, whereas low solvent-polymer affinity and large crystallization enthalpy favor solid-liquid separation. Solvent-polymer affinity and crystallization enthalpy were stated as the dominant parameters. In that study, all the interaction parameters (opposite of mutual affinity) were set to constant positive values. However, in this thesis, only the polymer-nonsolvent interaction parameter is positive (negative affinity), the other two are negative (high affinity), which can limit the transferability of the conclusions from that study to this thesis. The nonsolvent-polymer and solvent-nonsolvent affinities clearly changed as different nonsolvents were used. In this thesis, the solvent polymer and solvent-nonsolvent affinities did not change except for when DMSO was added to the solvent. These affinities decrease with increasing DMSO concentration in the solvent (see Subsections 2.4.2-3). The crystallization enthalpy should in theory be the same for cellulose but, in practice, could change as a function of crystallite size and the degree of crystalline order. The Flory-Huggins theory accounts only for equilibrium aspects, but the deciding parameter is often kinetics, which favors liquid-liquid over the slower crystallization that takes place in solid-liquid separations. Therefore, in some cases, liquid-liquid separation will come first but in the polymer-rich liquid phase, solid-liquid separation will follow.

2.2 Mass Transport

This section introduces the fundamental phenomena that generate the change in the composition of cellulose solutions, which induces coagulation upon immersion in a nonsolvent. An overview will be given of mass transport through liquid media, the effects of dissolved polymers and of additional solid phases, and the basic mathematics of diffusion. The mass transport of greatest interest to this thesis and treated herein is that of “small”

molecules, i.e. solvent, co-solvent, and nonsolvents, not polymers. The discussion is also limited to transport in a single dimension, although textile fibers are typically cylindrical in cross section. It is sufficient to treat the fundamental principles in a single dimension knowing that formulas are available for the translation into more complex geometries.

2.2.1 Diffusion

The random motion of molecules gradually reduces differences in chemical potential. In many cases, chemical potential is the same as concentration, which simplifies the diffusive process as a purely entropical one. However, in other cases there can be particular affinities and interactions between specific molecules that generate forces that guide the molecules according to enthalpic considerations. In such cases, the chemical potential is more complex and includes not just random motion but also the preferences of molecules for certain surroundings, such as water's distaste for oil. It will suffice to discuss concentration in this section, although it will be kept in mind that there can be additional complexities.

The random motion of a molecular species will always yield a net flow from A to B that is proportional to the difference in the numbers of molecules at A and B. The net flow will also be proportional to the rate at which molecules make random moves and inversely proportional to the distance between A and B. Adolf Fick made these conclusions as early as in 1855 and derived his equation, Eq. 2. [9]

$$\frac{\partial C}{\partial t} = D\frac{\partial^2 C}{\partial x^2} \qquad (2)$$

The equation states that the change in concentration within a volume element is the difference between the fluxes of in- and outgoing molecules. The fluxes are, as described above, the difference in concentration between neighboring elements divided by their distance times the rate, which is described by the diffusion coefficient, D.

However, diffusion coefficients can be a confusing issue, with several kinds used in different contexts. Diffusivity is the term used for the local mobility of a molecule in a small volume. This property can be measured with NMR techniques, in which nuclei within a certain volume element are tagged by giving them a nuclear spin. If measured on, e.g. water molecules in pure water, the term self-diffusivity (of water) is used. In more applied contexts, the net diffusion due to a concentration difference between A and B is measured, such as diffusion along a tube, across an interface, or through a membrane. In such cases, the "mutual diffusion coefficient" refers to the net flux of species x from A to B, which also depends on the movement of species y from B to A, due to the interdependence of all species in motion. However, these cases are generally complex due to the dependence of D on concentrations of both x, y, and other species. For this reason, it is often more appropriate to consider a mass transport coefficient, which provides an average value of *D*. [10]

2.2.2 Convection

Convective flow is the dominant mixing phenomenon in the nonsolvent that is outside immersed cellulose solutions. However, inside the coagulating solution, the cellulose

molecules resist convection with the hydrodynamic drag that they exert on any liquid moving through them. Still, if compound x is abundant at A and moves to B much faster than compound y, which is abundant at B, moves from B to A, the movements of x and y are interdependent. The accumulation of x+y at B causes the volume to expand, which in a fixed reference frame implies a convective flow of both x and y from B to A, as shown in Fig. 3. In many practical cases, this component of convection is not separable from the diffusive processes, which proceed simultaneously. The result is often a slightly increased "observed diffusion" of the slow component and a slightly decreased "observed diffusion" of the fast component. This effect actually constitutes much of the difference between diffusivity and mutual diffusion, as discussed in Subsection 2.2.1. The restricting forces of drag from larger less mobile molecules depend on the interface between the large non-mobile and the diffusing species. Expressions like Darcy's law can be used to quantify the convective-flow part of the mass transport, but require knowledge about the pressure gradient, which is not generally available. [10]

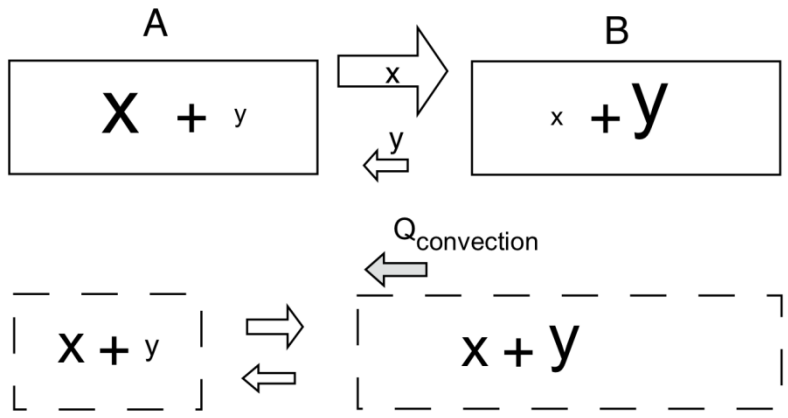

Figure 3. Example of how convective flow can arise as a consequence of unbalanced diffusive fluxes and counteract the diffusion imbalance.

2.2.3 Transient Diffusion

The immersion of a cellulose solution into a nonsolvent creates a large instability that is dramatic in terms of chemical potential, as diffusion and coagulation begin. From the start, there is a discontinuity at the solution-nonsolvent interface that diffusion and time will rapidly degrade into a continuous, gradually smoother concentration curve.In most practical situations on the macroscopic scale and over long time ranges, the initial difference declines exponentially. However, more complicated mathematical expressions are required to describe the process in detail at smaller length scales and for shorter times.

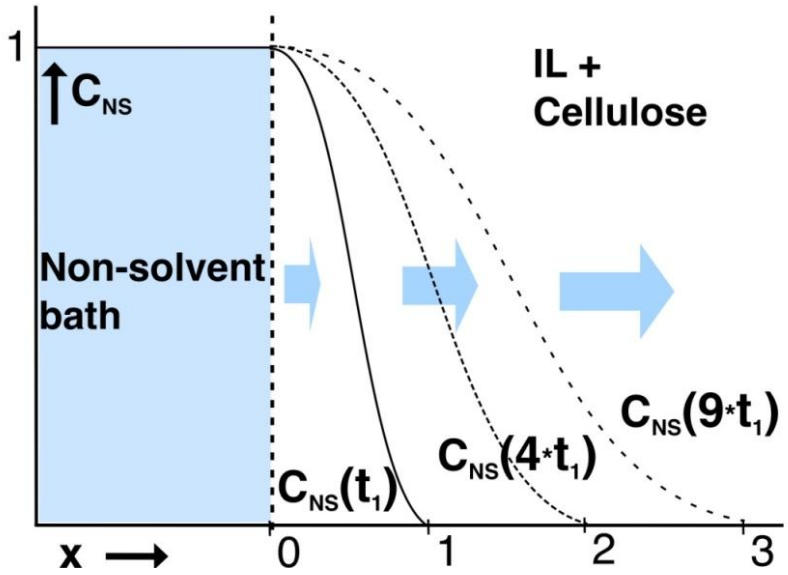

Figure 4. Example of transient diffusion of nonsolvent into polymer solution immersed in nonsolvent. Concentration on y-axis and depth into solution on x-axis. The elongating effect on concentration curves due to $C = f(z),\ z = x/(tD4)^{1/2}$ and the relation: x~$t^{1/2}$, exemplified by both curves and arrows.

The case described above for immersed solutions, with two volumes of different initial concentrations that are put in contact, is commonly referred to as the infinite slab problem (if D is constant)[11]. It combines Fick's differential equation, Eq. 2, with the initial and boundary conditions in Eqs. 3-4.

$$C(0,x) = 0,\ x \in [0\ \infty] \tag{3}$$

$$C(t,x)\ = 1,\ x < 0 \tag{4}$$

The difference between the analytical problem and real applied problems is the finite dimension of any real object. However, over time scales that are sufficiently short, finite objects can be considered as infinite, with regard to diffusion, without loss in precision. The analytical solution to the infinite slab problem, Eq. 5, is one of Ludwig Boltzmann's many discoveries and achievements. It predicts that the complementary error function, *erfc*, will be gradually stretched along the x axis at a rate that is ~$t^{-1/2}$.

$$C(x,t) = erfc\left[\, x/(tD4)^{1/2}\right] \tag{5}$$

The change of variables: $= x/(tD4)^{1/2}$, is a crucial step in the solution. This discovery is more generally useful than the *erfc* as the particular solution when D is constant. In processes where D varies, such as coagulation, the actual spatial concentration function does not have the shape of the *erfc*. However, in one-dimensional transient diffusive processes and if D depends only on concentration, the concentration function $f(z)$ can always be reduced to a function of only the dimensionless variable: $z = [x^2/(tD4)]^{1/2}$.[11] In our attempts to deduce the actual concentration functions inside coagulating cellulose solutions, it is crucial to

know that their shape is generally constant, although it becomes elongated with time, as shown in Fig. 4. The change of variable, $z = x/(tD4)^{1/2}$, is generally applicable and predicts the same type of stretching in space and development in time, whatever the shape of the function being stretched.

2.2.4 The effect of polymers in solution on small molecule diffusion

The diffusion of spheres that are significantly larger than surrounding molecules through small-molecule liquids follows the Stokes-Einstein relation, Eq. 6, in which T is the temperature, k_B is Boltzmann constant, r is the sphere radius, and η is the solvent viscosity.

$$D = \frac{k_B T}{6\pi\,\eta\,r} \tag{6}$$

However, the relation $D \sim \eta^{-1}$ is no longer valid when the diffusing entities, such as small molecules, decrease in size to a similar or smaller size than that of the molecules constituting the surrounding medium. It is replaced by a weaker dependence on viscosity, $D \sim \eta^{-2/3}$. [12]

There is no upper limit to the increase in the macroscopic viscosity of a solvent due to the addition of a polymer. However, the effect on small molecule diffusivity is always much smaller because small molecules can pass between larger obstructing polymer coils. The obstructive effect of the immobile polymers on D_s generally only reduces it to $\sim 1/2$ relative to the pure solvent, even at polymer concentrations of 30-40 wt%. D_s follows a slow exponential decline according to Eq. 7, where k is a small constant, C_p is the polymer concentration and $D_{s\,0}$ is the diffusivity in a pure solvent.

$$D_s = D_{s\,0} \exp\,(-\,kC_p\,) \tag{7}$$

Generally, D_s is not affected by the DP or cross-linking of the polymer. There are two circumstances in which polymers can give a much larger effect on D_s. The first circumstance is if C_p is very high, typically >40 wt%. Then there is no longer an unaffected continuous solvent phase between the polymers. With only one or two solvent molecules between the polymer chains, there is no longer an unaffected normal solvent phase through which to diffuse. The whole volume is essentially made of either polymers or solvent molecules in contact with the polymers, and those solvent molecules have much lower mobility than "normal" solvent molecules. Thus, for C_p >40 wt%, Eq. 7 is replaced with Eq. 8, where b, the exponent on C_p, can be as high as 3.8. This illustrates the dramatic effect observed when the solvent phase becomes gradually less continuous. [12]

$$D_s = D_{s\,0} \exp\,(-kC_p{}^{b}\,) \tag{8}$$

The second circumstance is if there are strong attractive forces between the polymer and the diffusing small molecules. The interaction between a mobile small molecule and an immobile polymer can considerably reduce the mobility of the small molecule. This effect has been observed for [C_2mim][OAc] with dissolved glucose and cellulose [13, 14]. The decrease in D_s

depends only on the number of OH groups present on the carbohydrates, regardless of the covalent bonds between glucose units in cellulose. The mass of glucose is sufficient to retard the smaller OAc anion through an H bond between the two compounds. The H bonds are broken and rearranged before the glucose has moved anywhere with the solvent molecules attached, regardless if the glucose is a monomer or part of a polymer. This constitutes an explicit example of how very local conditions control small-molecule diffusion, which tends to disregard long range connectivity.

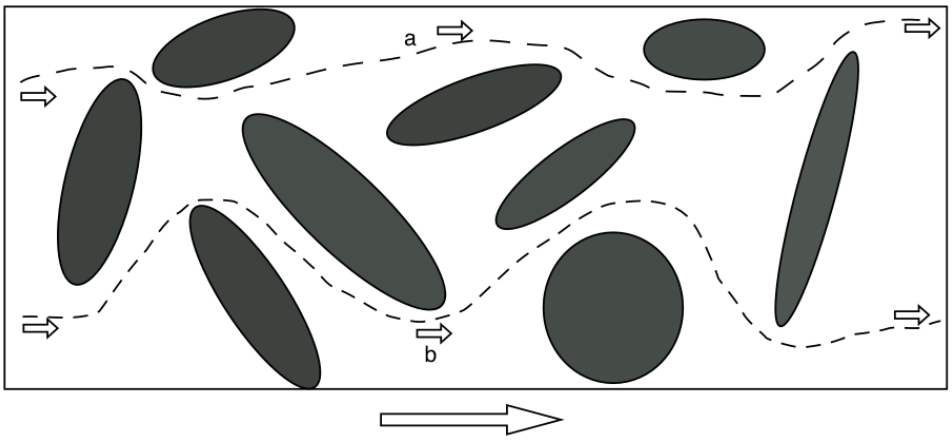

Figure 5. Tortuous paths for diffusion through dual phases. Note that the paths can vary in length as a function of the shapes and the orientations of the impenetrable domains.

2.2.5 Single versus dual phase diffusion

In heterogeneous material that is composed of multiple phases X and Y, D_s can be very different in the two phases. The difference is often so large that diffusion through the phase with lower D_s, e.g. Y, can be neglected. In addition to not contributing to the mean D_s of the whole volume, Y can impede diffusion through X by means of several mechanisms. First, the diffusive path through phase X is extended when winding around the domains of Y, as shown in Fig. 5. The figure shows two different paths, *a* and *b*, in which this effect, tortuousity, depends on the shape of the domains of Y and on the volume fraction of the domains. Flat and continuous shapes can generate a large diffusive resistance, whereas cylindrical and spherical shapes generate only marginal effects unless the volume fraction of Y is very large. Tortuousity typically affects all compounds equally because it is due to purely geometrical aspects. Second, Y may absorb or adsorb certain small-molecule compounds due to specific interactions between them and the other compounds of Y. If a certain compound is more soluble in Y than in X, only the lower concentration of its molecules in X will contribute to the diffusion of that compound. If Y is a crystalline phase, the solubility of other molecules is generally not significant, but there may still be adsorption on its surfaces, which can be in the order of 10^2-10^3 m^2/g in cellulose materials [15]. Either type of sorption is typically selective of certain compounds over others and depends on the properties (e.g. polarity) of both X and Y. [16]

2.3 The Compounds

The compounds involved (see Fig. 6) and their properties are presented in this section. The compounds are grouped based on their roles relative to other compounds: cellulose, [C_2mim][OAc] (solvent), DMSO (cosolvent), and nonsolvents. The properties that affect the interactions of each compound with itself and with the other compounds are of particular interest. Closely related compounds, such as other alcohols, can also be of considerable interest for understanding the interactions of the nonsolvents in particular. Table 1 contains a selection of data that can generate some understanding of these compounds and how they behave.

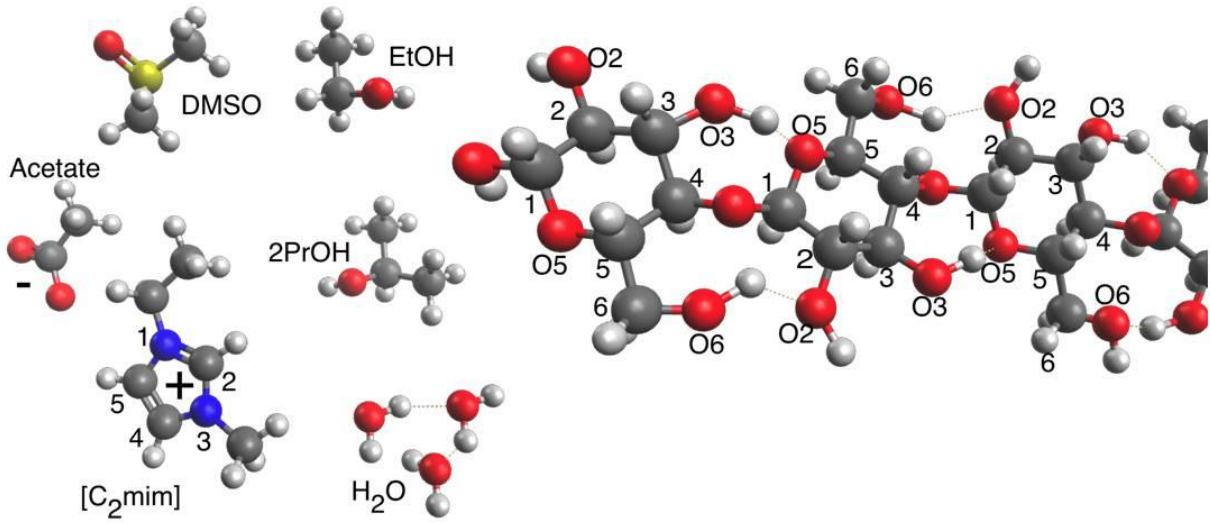

Figure 6. The molecules involved: solvent ([C_2mim][OAc]), cosolvent (DMSO), and nonsolvents on the left; and three AGUs of a cellulose chain on the right. Certain atoms mentioned in the text with reference to H*x*, O*x*, or OH*x* are numbered according to the number, *x*, of the carbon they are closest linked to.

2.3.1 Cellulose

Molecule

Cellulose is a linear polymer of β-D-glucopyranose monomers in chair conformation linked through a 1-β-O-4 glycosidic bond. These monomers with a M_W of 162.14 g/mol and the formula $[C_6H_{10}O_5]_n$ are generally referred to as anhydroglucose units (AGUs). The glycosidic bond rotates each monomer by 180° around the chain axis (see Fig. 6) relative to the neighboring monomers. This results in a straight polymer, unlike, e.g. amylose, which has an inherent bend due to its 1-α-O-4 bond. The rotation around a glycosidic bond is not predetermined in itself, but in the case of cellulose, the intramolecular OH3···O5 and OH2···OH6 H bonds, which are present on each side of the glycosidic covalent bond, strongly enforce the 180° rotated confirmation. As a consequence of these intramolecular H bonds locking the glycosidic-bond rotation, the chain becomes straight and stiff, as long as the H bonds are maintained. [17]

β-D-glucopyranose is constructed in such a way that when bonded 1-β-O-4, its OH groups are located at the periphery of its ring plane. The position and direction of OH6 is more variable than those of OH2 and OH3, which enables slightly less flat conformations. The peripheral positions of the OH groups still leave the glucose-ring planes hydrophobic with low polarity. However, the edges, on which OH groups are positioned, are hydrophilic and polar. The three OH groups are also the primary points of interaction and reaction with surrounding chemical species[18, 19]. Also the ring oxygen, O5, is a strong HBA base, probably stronger than most monohydric alcohols if it is assumed that the glucose O5 is similar in HBA basicity to the ring oxygen in tetrahydropyran. The proton affinity, PA, of O5 has also been estimated to be 787kJ/mol, similar to the PA of 2PrOH (790kJ/mol), with density functional theory simulations on β-D-glucopyranose in the gas phase[20]. The PAs of the OH groups of glucose have also been calculated. The PAs of OH2 and OH3 were 755 and 760 kJ/mol, which was slightly below the 770 kJ/mol calculated for EtOH, the reference point. The OH6 had a lower PA, which could not be evaluated due to transitions to OH4 (741 kJ/mol).Cellulose chains are asymmetric, not just with regard to their cross section, but also along the chain. Each AGU monomer appears differently if observed up or down the chain length.

Solid

Cellulose can be arranged in four crystalline allomorphs, of which only two are of practical interest: allomorph I and II. Cellulose is created in nature by enzyme clusters that extrude the molecules in parallel. This allows them to organize in very long and slender crystallites with relatively square cross sections that are composed of 30-1000 chains, depending on the origin [21]. The crystalline allomorph of this material is cellulose I, which is a technical solution that has been oligopolized by plants, certain very primitive animals, and bacteria. It has various particular characteristics that will not be further discussed here, as the starting point of this thesis is dissolved cellulose from which cellulose I cannot be reproduced. Because cellulose II is the most thermodynamically stable allomorph, all cellulose that has been dissolved and precipitated is in this form. In cellulose II, anti-parallel chains are stacked on their hydrophobic planes ([011]) with 4.4 Å distances between (see Fig. 7). The stacks are assembled in the $[0\bar{1}1]$ direction, which is roughly perpendicular to the [011] plane, with a stagger so that anti-parallel chains alternate in the same [011] plane[22]. The positions of chains can be presented and rationalized in terms of planes in two roughly perpendicular directions. However, the patterns of H bonds in cellulose II are more complex[23]. The H bonds are not limited to pairs of H-bonded OH groups, but constitute small assemblies of numerous OH groups. In these networks, individual OH groups act as both donors and acceptors in parallel, and protons can involve multiple acceptor O atoms. The H-bond network is most apparent between anti-parallel chains in the same [011] plane. It involves mainly O3, O5, and O6 in both intra- and intermolecular H bonds. However, the stagger of neighboring stacks is not a full [011] plane, but rather ~¾ of a [011] plane, which allows H bonding also to the parallel chain ¾ of a [011] plane down in the neighboring stack. Those H bonds involve mainly O2 and O6 and appear to be less interconnected to other OH groups. The result is a network of H bonds in both of the directions that are perpendicular to the chains. This network enhances considerably the stiffness of the single molecule when it is integrated into a crystalline structure. The hydrophobic interactions between glucose ring planes have been assigned some importance as a cohesive force for cellulose structures.[24]

Hydrophobic pairing energy per AGU in water has been estimated to be ~8 kJ/mol in molecular dynamics simulations [25]. While significant it is less than half the energy of one $H_2O\cdots HOH$ bond.

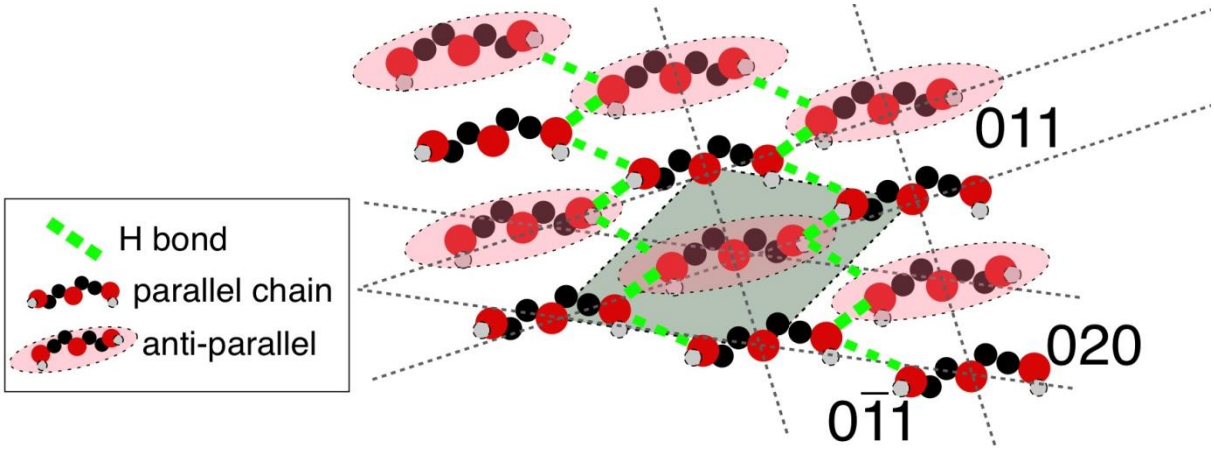

Figure 7. A part of the cross section of a cellulose II structure shows how H bonds connect mainly between parallel and anti-parallel chains in the same [011]; and also between parallel chains in the same [020] plane. The unit cell is marked in grey.

The crystalline peaks in XRD spectra of regenerated cellulose are often relatively broad and overlap with a broad peak that covers most of the upper part of the spectrum. The broad peak is generally attributed to "amorphous" cellulose [17]. However, it is not very clear what "amorphous" actually means in a cellulose context. It is probably not the same as amorphous thermoplastic materials solidified from melts of flexible polymers, due to the stiffness of cellulose chains and their tendency to organize at least relative to their nearest neighbors. It is, therefore, thought that the molecules are generally well aligned and coordinated with their neighbors but not with chains that are further away. How far the organizing stretches varies throughout the material, from complete crystalline order in nm-sized crystallites to the local alignment of a few chains. This is generally called a fringed-micelle structure, but it is rarely specified more exactly what the term represents. For example, the evaluation of crystalline index (crystalline versus amorphous volume fraction) by comparing the crystalline and "amorphous" WAXS-spectrum peak heights [26] is one indication that many scientists envisage a much more distinct border between "amorphous" and crystalline material.

In solution

In order to achieve dissolution, the H bonds of cellulose must be broken. Very strong HBA bases can break them by forming H bonds to cellulose that are stronger than the cellulose-cellulose H bonds. Many such bases have a negative charge, which means that the cellulose becomes charged. Cellulose-cellulose H bonds can also be broken by the protonating or deprotonating action of a very strong acid or base, which also adds electrostatic charges to the OH groups. Either way, this means that there are strong interactions between the solvent molecules and cellulose in the dissolved state [27]. The dissolution of cellulose is generally exothermal, and sometimes also the precipitation must be exothermal in order to create a sufficient driving force to break the solvent-cellulose interaction. The OH2 and OH6 are the OH groups that are primarily involved in intermolecular H bonds and need to be broken in order for dissolution to occur. They also interact most with the solvent, whereas OH3 tends to

be less active in either reactions or temporary interactions, due to its tendency to H bond intramolecularly to O5[23, 25]. The pK_a values for β-D-glucopyranose have been estimated with density functional theory simulations [20]. The pK_a values calculated for the OH groups of β-D-glucopyranose varied significantly in these simulations: $pK_{a\ OH1}$ =14.08, $pK_{a\ OH2}$ =18.92, $pK_{a\ OH3}$ =18.11, $pK_{a\ OH4}$ =18.06, $pK_{a\ OH6}$ =20.65. However, the calculation of solvation energies incurred significant overestimation as the experimentally determined $pK_{a\ D\text{-}glucose}$ is 12.5 [28]. A more reasonable set of conclusions from these results is: pK_a values are reduced by adjacent OH groups, such as for OH1, OH2, OH3, and OH4; OH1 on the anomeric carbon is the most acidic by a margin; and OH6 is less acidic than the others. The OH1present on glucose in the simulations, is not present on the AGUs of cellulose, where OH1 has been replaced by the glycosidic bond. Therefore, the pK_a of cellulose should correspond to $pK_{a\ OH2} \approx pK_{a\ OH3}$, at least before the OH3-O5 H bond is considered. There is no apparent reason for these values to exceed the pK_a =15.1 of ethanediol or to fall short of the pK_a =14.1 of glycerol, which have been experimentally determined[28]. Whereas $pK_{a\ OH2}$ and $pK_{a\ OH3}$ are expected in the range of 14-15, $pK_{a\ OH6}$ is probably similar to the pK_a of MeOH or EtOH at 15.5[28] (other references give $pK_{a\ EtOH}$ =15.9[29]). No reported numbers have been encountered for HBD acidity during the preparation of this thesis. Therefore, the best assumption is that HBD acidity is similar to ethanediol or perhaps 2,3-butandiol. The acceptor number, AN, which is closely related to HBA basicity, has been investigated for cellulose acetates of variable degrees of acetylation[30]. The AN basicity of underivatized cellulose was estimated to be less than that of glycerol but larger than that of MeOH in that investigation. Although specific data on cellulose is not available, the examples and comparisons above indicate that cellulose is more prone to interact with polar molecules and ions through H bonds or deprotonation than monohydric alcohols, about as prone as diols, but genereally less prone than glycerol and monosaccharides.

The existence of anisotropic (liquid crystalline) phases in cellulose solutions has been verified in several solvents [31, 32]. In liquid crystalline solutions, cellulose chains are aligned with their closest neighbors. This phenomenon of short range order arises at high concentrations due to the stiffness of the dissolved polymer chain. The molecular situation can essentially be compared to a bunch of toothpicks confined in a box. The box, which corresponds to the volume of solvent and polymer, needs to be much larger to contain all toothpicks if they are randomly oriented, crossing each other at angles, than if they lie more or less parallel to each other. In most solvent systems, liquid crystalline phases cannot be used in practice because the concentrations and viscosities, above which they form, are too high. Nevertheless, liquid crystalline phases are clear manifestations of the large chain stiffness of dissolved cellulose. The persistence-length (the smallest length between monomers of non-correlating orientations) of cellulose varies between 8 and 25 nm for different solvents[33]. There are several factors that can cause these large variations. If a polymer carries charges due to the deprotonation of OH groups or H-bonded ions, the chains can be straightened for electrostatic reasons, which would stiffen its back-bone. If the solvent breaks the intramolecular H bonds, the solvation effect increases the rotational freedom of the glycosidic bond between monomers, which reduces chain stiffness. Measurements of the hydrodynamic radius of dilute cellulose in $[C_2mim][OAc]$ indicate that the chain stiffness in $[C_2mim][OAc]$ is in the lower range of persistence-lengths for cellulose [34]. However, assuming that the relatively low

stiffness of the chain is due to the solvation of intramolecular H bonds, the chains could be much stiffer at higher cellulose concentrations, at which measurements are not possible.

Table 1. Important properties of compounds from CRC Handbook (online), unless marked with a parenthesis or referenced. *ββ* and *αα* are solvatochromic indicators of HBA and HBD property, similar to thoe Kamlet-taft approach. pK_{HB} is also a measure of HBA basicity (like *ββ*), but with another probe molecule. [TBA][OAc] is tetrabutylammonium acetate, which does also dissolve cellulose, and should have properties similar to [C_2mim][OAc]. ΔH_{vap} $(C_nOH - C_n)$is the difference in ΔH_{vap} between an alcohol and its corresponding alkane.

	[C2mim][OAc]	**DMSO**	**H_2O**	**MeOH**	**EtOH**	**2PrOH**	**1BuOH**	**Et(OH)2**
M [g/mol]	(170)	78.13	18	32.04	46.07	60.1	74.1	62.7
μ [mPas]	(120) [35]	1.99 (2.47)[36]	0.89	0.54	1.07	2.04	2.54	16.06
D [10^{-10} m^2/s]	(0.08) [35]	(7) [35]	(22.3) [37]		(10.6) [38]	(6) [38]		
ΔH_{fusion} [kJ/mol]		14.37	6.01	3.215	4.931	5.41	9.37	9.96
ΔH_{vap} (25C) [kJ/mol]		43.1 (at T_b)	43.98	37.43	42.32	45.39	52.35	63.9
T_b [C]		192	100	65	78	82	118	215
ΔH_{vap} (C_nOH - C_n) [kJ/mol], (25C)					37	30	31	58
Log K_{OW}	-(2 – 2.5) [39]	-1.35	(-1.38) [40]	-0.74	-0.3	0.05	0.84	(glucose - 2.8) [41]
pK_{HB} [42]	5.6 ([TBA][OAc])	2.58	0.64	0.82				
ββ [43]		0.88	0.35	0.47	0.48	0.56	0.48	0.78
αα [43]		0	0.82	0.43	0.37	0.33	0.37	0.58

2.3.2 [C2mim][OAc]

[C_2mim][OAc] is one of countless possible combinations of an organic cation with an anion that form a low-temperature melting salt, an ionic liquid (IL). The low melting points of ILs are achieved by increased distances between oppositely charged ions, which reduce the electrostatic attractive force (ionic bonds) between the ions. Fundamental electrostatics establishes that the ionic force is $\sim r_{an-cat}^{-2}$, which means, e.g. that doubling the interionic distance, or bond radius, implies reductions in bond energy and in melting temperature in the order of 4 times. Actually 4 times is about the difference, in Kelvin, between the melting temperature of a common salt like NaCl and ambient temperature, at which [C_2mim][OAc] melts. However, steric factors are also important parameters. They can limit the efficiency of

packing in the crystalline state relative to the molten state. Numerical modeling has also shown that the interaction between anions and cations can be a mixture of ionic and H bonds, which can reduce the melting point by reducing the free energy of the molten state [44, 45].

Being composed of ions, ILs are polar substances, but the polarity of specific ions can still vary significantly so that some ILs are even relatively hydrophobic[46]. However, [C_2mim][OAc] has a very hydrophilic character, as is indicated by its octanol-water partition shown in Table 1. Acetate ions are primarily responsible for this, but the [C_2mim] ion is also hydrophilic, being a derivative of methyl-imidazole, which is miscible with water. Longer alkyl chains can replace ethyl to make the IL less hydrophilic, but long alkyl chains are not favorable for cellulose dissolution. The [C_2mim] cation (see Fig. 6) interacts with the anion through the imidazolium ring plane, which maximizes the electrostatic ionic bond, and by H bonding primarily through H2 and second through H4 and H5. It has been shown that an additional methyl group can replace H2 to reduce the acidity of H2 and prevent unwanted reactions at C2. This change reduces the H bonding between ions to some extent but C4 and C5 largely replace C2 as HBD.

Being salts, ILs also have very high vapor pressures, which have generally been presented as an advantage. However, high vapor pressures complicate the removal of non-volatile non-process elements. Instead of evaporating at elevated temperatures, ILs can degrade through side reactions. A wide spread of degradation onset temperatures has been reported since the initial interest in IL processing of cellulose. Some current reports indicate long-term stabilities not much higher than ~100°C for many IL cellulose solvents[47]. This is problematic because of the need to remove essentially all non-solvent, particularly water, which evaporates at about that temperature. Another problem is the viscosities of ILs, which are high but would be lower at higher temperatures if they were admissible. Viscosity can be particularly problematic for dissolution of cellulose, because it delays the mixing of the components. Therefore a common procedure adopted from the lyocell process is to mix the solvent with a nonsolvent and then add cellulose. The nonsolvent is evaporated to activate the solvent. At that point the solvent has already been well mixed with the cellulose with the help of a reduced viscosity in the ternary mixture. With this method cellulose concentrations as high as 28 wt% can be obtained[31]. However such solutions would require high temperatures to be filtered and extruded. Fortunately, cosolvents can be added to reduce solution viscosity at the expense of a slightly lower cellulose solubility[48]. The viscosity of ILs typically decreases exponentially with increasing additions of low-viscosity solvents, which can make even a small addition useful.

[C_2mim][OAc] and several other ILs are exotic, hydrophilic solvents with an impressive capacity for dissolving cellulose, due to their strong BHA basicity, but ILs are not without drawbacks and limitations.

2.3.3 DMSO

A rare set of properties is combined in DMSO, which makes it suitable as a cellulose-IL co-solvent. It has very high polarity, no acidic hydrogens, and a very strong basicity. The combination of the central sulfur atom, which has a relatively large electron cloud and the double-bonded oxygen atom, which keeps its electrons much more densely packed, gives DMSO a very strong preference for solubilizing cations over anions. It is often used with strong bases to deprotonate very weak acids like OH groups. However, pKa values in DMSO are generally very high compared to other solvents. This is because although its interaction with protons is very strong, the remaining anion, conjugate base, is poorly solvated in DMSO [49]. DMSO has a high boiling point at 190°C and melts at 18°C. No adverse health effects have been reported, unlike most other polar aprotic solvents, such as NMP, DMAc, and DMF. The dipole moment of DMSO is 4.3 D, its pK_a is 31.3, and its pK_b is 0.911. The viscosity of DMSO is similar to the much less polar but geometrically similar 2PrOH. [36]

2.3.4 Nonsolvents

All nonsolvents of interest to this thesis can be described as R-OH, where R can be H (water) or an alkyl chain (acohol). Thus, a central question is the effect of different R on the properties and interactions of the nonsolvent. Water generally stands out from the alcohol nonsolvents because of its double HBD capability. An increase in the alkyl-chain length of alcohols generally reduces the density of electrostatic charge on the hydroxyl groups by the dispersion of charge to the closest atoms. Therefore, protonation and deprotonation in the gas phase is more energetically favorable for alcohols than for water, and protonation and deprotonation in the gas phase is most favorable for long alkyl chains and for secondary alcohols. However, the effect is limited to the closest atoms, which often inverts the order of proton affinities in solution (compared to the gas phase). This effect gives water the second lowest pK_a, after MeOH, in 2PrOH [50] and in aqueous solutions. However, all the pK_as in DMSO [20] are very high and in the order: MeOH, EtOH, 2PrOH, water, t-BuOH. The main reason for this is that DMSO solvates more hydrophilic and smaller anions better. Water probably H-bonds much better to DMSO than DMSO solvates OH^-, which inhibits deprotonation. The fundamental properties of a molecule and its respective deprotonation and protonation products, as observed in the gas phase, are generally overwhelmed and obscured in solution by interactions with neighboring molecules.

Although gas-phase proton reactions are neat measures from a theoretical perspective, they do not give the whole picture, which requires complementary information. Boiling and melting points, and the enthalpies of these phase changes give indications of the strength of intermolecular forces. Octanol-water partition coefficients are useful indicators of the compound hydrophobicity or hydrophilicity. HBA basicities and HBD acidities, indicate which other compounds a specific compound can H bond to and how strongly. The increases in boiling points for longer alkyl chains show that van der Waals forces are not negligible for these alcohols. A comparison of $\Delta_{vap}H$ between alcohols and the corresponding alkanes (see $\Delta_{vap}H\,(C_nOH - C_n)$ in Table 1) suggest a contribution from H bonds in the order of 30 kJ/mol and a significant remaining binding energy due to van der Waals forces. H bond acidities and basicities show that water is far more H-bond acidic than the monohydric alcohols, even more

than diols. This is also reasonable with regard to the trends in $\Delta_{sol.DMSO}H$ of the different nonsolvents presented below in Subsection 2.4.3, since DMSO is a very strong HBA. Water is a weaker HBA base than alcohols, which are all similar except for 2PrOH, which is slightly stronger (see Table 1). However, low HBA basicities measured at infinite dilution do not preclude that water clusters in aqueous solution are more efficient HBAs than the alcohols[1] [42]. The trends in K_{OW} reflect the differences in boiling points, which show that water is, expectedly, much more hydrophilic than alcohols.

2.4 Interactions

The following subsections are devoted to the most important interactions between specific compound pairs. However, H bonds dominate most of these interactions, which motivates a brief introduction to the vast subject of H bonds. Certain aspects, such as the effects of net charge and symmetry on the strength of H bonds, are particularly important to our subject. Hydrogen bond donor (HBD) acidity and hydrogen bond acceptor (HBA) basicity are properties that govern these interactions. It was clarified in Subsection 2.2 how such properties can affect mass transport. Most importantly, however, is that they control the mutual affinities and solubilities of one compound in another, which can determine the type of phase separation. Direct information about these mutual affinities is not generally available, but certain related properties, such as mixing enthalpies, interaction energies evaluated in molecular dynamics or quantum modeling, activity coefficients, relative vapor pressures, and solvatochromic H bond indicators, give some useful indications.

Cellulose (polyol), EtOH, and 2PrOH, which are alcohols, and water can be either HBDs or HBAs. The HBA function of cellulose and nonsolvents is mainly of interest for the interactions between nonsolvent and cellulose. Due to the HBA base nature of both acetate and DMSO, HBD acidity is the most interesting property of cellulose, alcohols, and water. Consequently, the subsections on specific interactions are grouped as follows: [C_2mim][OAc] – (Cellulose & Nonsolvent), DMSO – (Cellulose & Nonsolvent) and Cellulose – Nonsolvent.

2.4.1 Hydrogen bonds

The polar and hydrogen bond-prone character of cellulose and its solvents motivates a closer look at the hydrogen bond. The positive charge of a proton (H^+) that is attached to a particularly electronegative atom (A), such as fluorine, oxygen, or nitrogen, is poorly shielded by the electron pair that bonds it to A. This poor shielding makes it attract other atoms with a negative electric charge (nucleophile atoms or ions) in its surroundings. As one of those molecules (B) approach the proton, the electrostatic energies of both H^+ and B are reduced. The repulsive electrostatic forces between A and B act over a longer distance (2-4Å) and are weaker than their respective attractive forces to H^+. Consequently, an H bond, $AH^+\cdots B$, is formed, and the associated net reduction in enthalpy of ~10-160kJ/mol (depending on A and B) is dissipated as heat to the surroundings. The proton remains partially shielded by the

[1] HBA and HBD measurements are performed in dilute solutions in media which does not H bond. Therefore cooperative effects of multiple molecules and complexes cannot be observed.
[2] ¾ is the roughly estimated difference between CB and two AGUs, based on the different numbers of available OH groups in each (4 and 3).

covalent-bond electrons, a factor that reduces the effective net charge that is sensed by B. Therefore, the effective charge associated with H^+ is typically not a full elementary charge $-e^-$, but a fraction, δ^+, of $-e^-$. The size of δ^+ increases with the electronegativity of A and is the primary decisive parameter for the strength of an H bond.

There are also minor redistributions of electron clouds: B toward the proton and a slight withdrawal of the electrons of A from the proton. The redistribution of electrons is less important than the translation of the proton, but their redistribution generally does not stop at atom A and B. This polarizing effect on the electron clouds continues into A and B's neighboring atoms of the same molecule. Therefore, if H bonds are numerous and allowed to form chains ($AH^+\cdots$ $AH^+\cdots$ $AH^+\cdot\cdot$), they can be strengthened by this polarizing effect. This is the case with water and is probably the case with solid cellulose [23, 25].

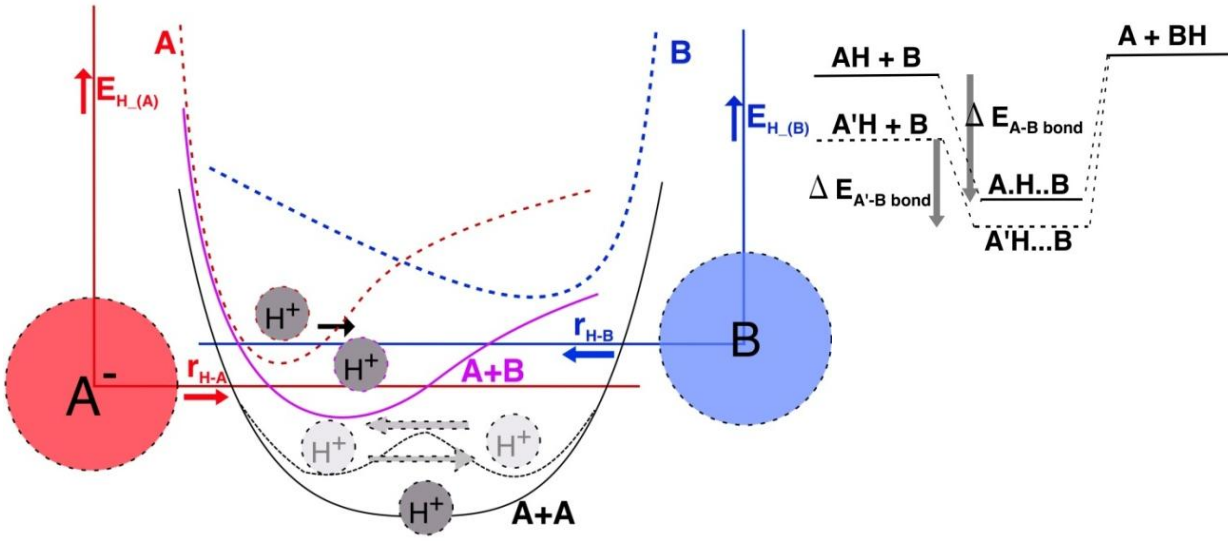

Figure 8. Left: two electronegative atoms, A and B, and their electrostatic fields (red & blue) approach each other, due to a common attraction to H^+. Together, the fields form the potential "A+B" (purple) that provides a deeper and wider, more preferable, potential (well) for H^+. If the electronegativity of B is close to that of A^- (without its H^+), symmetric even more preferable potentials can be formed (black, grey). R**ight**: the effect of bond symmetry is demonstrated by the grey arrows, which represent the bond energies of more and less symmetric atom pairs (A, B).

The covalent bond A- H^+ is always stronger and, thus, shorter than the distance H^+-B, but if the nucleophilicity of B increases or that of A decreases, the covalent distance A-H^+ becomes longer and H^+-B becomes shorter. More symmetrical H bonds are generally stronger bonds. In some sense, this is similar to a chain not being stronger than its weakest link. One approach to this aspect is to consider A and B as two bases that, in the presence of H^+, can form $AH^+\cdots B$, $A\cdots H^+B$, AH^+ + B, or A + H^+B, as in Fig 8, Right. The H bond strength would then be the enthalpy difference between the lowest energy of the H-bonded states ($AH^+\cdots B$ or $A\cdots H^+B$) and the lowest energy of the non-bonded states (AH^+ + B or A + H^+B). For instance, if A is a stronger base (has a higher proton affinity) than B, then $AH^+\cdots B$ and AH^+ + B will be the lowest states. The energies of both of these states will be reduced if A is exchanged for an even stronger base. However, the non-bonded state is reduced the most, which gives a reduction in H bond strength. This issue of the symmetry of H bonds and the balance of bases

highlights an important difference between strong ionic H bonds, to which a net charge is associated, and the weaker "normal" H bonds between neutral molecules. In the latter case, the remaining donor molecule without H^+ would be a negatively charged base that is much stronger than a neutral acceptor. As a consequence, such bonds are generally limited to <60 kJ/mol. However, in the former case, the base, A, that is hypothetically left behind by H^+ would have about the same charge as the acceptor B. H bonds HF ⋯ H_2F^+, H2O ⋯ H_3O^+, or H_2O ⋯ OH^- are examples of symmetrical bonds that can instead be described as A··H^+··A. These examples are not just symmetrical but even centrosymmetrical, which means that the electrostatic potential field sensed by the proton has a single minimum and places the proton halfway between the H-bonded nucleophiles. Such bonds are typically >120 kJ/mol. In this thesis, the anionic bonds between [OAc^-] and the HBDs (cellulose and nonsolvents) are not quite as symmetrical, but are certainly much stronger than the neutral bonds between the other compounds present. [51]

2.4.2 [C_2mim][OAc] – Cellulose & Nonsolvent

Among the infinite combinations of ILs, [C_2mim][OAc] is one of much fewer ILs that can dissolve cellulose to significant concentrations. Solutions of 28 wt% cellulose can be obtained in pure [C_2mim][OAc] [31], which corresponds to about 2.5 [C_2mim][OAc] per AGU. A ratio of 1.5 [C_2mim][OAc] per AGU is obtainable[52] in [C_2mim][OAc] diluted with DMSO. Molecular dynamics simulations of 1.5-3.5 wt% cellulose in [C_2mim][OAc][53] predict, on average, 2.5-2.8 H bonds for each AGU (presumably involving one [C_2mim][OAc] per H bond). The anion is a relatively strong base and a very potent HBA, which H bonds to most OH groups, such as those of cellulose[54], EtOH [55], or water[56]. Modeling (ab initio) of the Ac^-⋯HO-cellulose bonds has predicted a strength of about 60kJ/mol for each of these bonds [53] , which is much more than the 25kJ/mol of each cellulose-OH⋯OH-cellulose bond. Because this predicts a negative enthalpy of dissolution that should be sufficient by itself, it is reasonable to consider anion-OH-cellulose H bonds as the primary solution-stabilizing mechanism. However, molecular dynamics simulations have predicted additional interactions, a mixture of H bonds and Van der Waals forces, between cation and cellulose in [C_2mim][OAc] solutions of 1-3wt% cellulose [53]. That study has also found that Van der Waals forces constitute ~3/4 of the interaction-energy contribution from cations. Thus, the total van der Waals interaction energy (exclusively from the cation) would be more than 1/5 of the total interaction energy between [C_2mim][OAc] and cellulose. This is a surprisingly large number given that specific stacking of glucose and [C_2mim] rings was not observed in the simulations. The total [C_2mim][OAc]-cellulose interaction energy was estimated to ~300 kJ/mole (AGUs) , which was ~100 kJ/mole more than was estimated for cellulose and water, which is not a solvent. Values for the enthalpy of dissolution, $\Delta_{sol}H$, give a more holistic view, because $\Delta_{sol}H$ takes into account the enthalpies of both the dissolved state and the pure solvents and cellulose. However, experimental values of $\Delta_{sol}H$ are only available for cellobiose (CB) and only in [C_4mim][OAc] [57] (butyl instead of ethyl in [$C_n$mim] cation). CB is the β1-O-4-bonded dimer of D-glucose, which is often used to model cellulose to study solvent interactions because it dissolves more easily than cellulose. It can be dissolved even in solvents that do not dissolve cellulose. However, there are some significant differences between CB and cellulose that must be taken into consideration, such as that CB has 4 OH groups per AGU instead of 3, and the extra OH groups are OH1 (more acidic [20]) and OH4,

which can add to the acidic character of OH3. Therefore, $\Delta_{sol}H$ for cellulose is likely to be less than $\Delta_{sol}H$ for CB, probably ~3/4 of $\Delta_{sol}H_{CB}$ [2]. $\Delta_{sol}H_{CB}$ in pure [C_4mim][OAc] ([C_4mim] instead of [C_2mim]) was determined to be -38 kJ/mol(CB). However, in consideration of an unsubstantiated assumption in the method used[3], it appears that the $\Delta_{sol}H_{CB}$ determined in that study [57] for a number of ILs was actually about ~20 kJ/mol lower (e.g. - 55-60 kJ/mol in [C_4mim][OAc]; ~ -50kJ/mol in [C_4mim][DEP]; and ~ -30kJ/mol in [C_4mim][Cl])[4]. Assuming that ¾ of these values correspond to two AGUs would give rough estimates for $-\Delta_{sol}H_{AGU}$ of: 20-22 kJ/mol (in [C_4mim][OAc]), ~ 19 kJ/mol (in [C_4mim][DEP]), and ~11 kJ/mol (in [C_4mim][Cl]).

A central parameter in this thesis is the relative order of interactions between [C_2mim][OAc] and each HBD compound (nonsolvent or cellulose), and the following is interesting reported data regarding the nonsolvents. Water is particular with regard to its H bonds to carboxylate ions, which are ~100kJ/mol[51, 56], e.g. compared to ~60kJ/mol for cellulose-OH-acetate H bonds. The difference in interaction energy is mainly due to the two H of water, which can both interact either with two different [OAc^-] ions in concentrated IL solutions[56] or with a single [OAc^-] ion if in gas phase[51]. The mixing enthalpy of water in [C_2mim][OAc], $\Delta_{sol.\ [C2mim][OAc]}H_{water}$, is about 35kJ/mol [56]. Computed predictions of the relative vapor pressures of water-ethanol and water-2PrOH azeotrope solutions mixed with [C_2mim][OAc] in weight proportions of 35:65 have shown that the relative volatility is enhanced >35 times for 2PrOH and >16 times for EtOH [58]. Different cations have also been compared and have shown a smaller relative volatility for more hydrophobic cations with longer alkyl chains ([$C_n$mim]). These results indicate much stronger interactions between water and [C_2mim][OAc] than between [C_2mim][OAc] and EtOH or 2PrOH (weakest). This order would be expected based on the values for HBD acidity ($\alpha\alpha$ in table 1), which are considerably lower for alcohols than for water and decrease with the length of the alkyl chain. A key objective of this section is to put an order to the interactions with [C_2mim][OAc] of different HBD compounds. Perhaps the best measure to predict this order would be the octanol-water partition, $K_{OW,}$ (see Table 1). Glucose and [C_2mim][OAc] are both >100 times more concentrated in the hydrophilic phase and relatively similar on this scale, whereas water (~30 times) is in-between [C_2mim][OAc] and MeOH, which is considerably less selective of the water phase. The alcohols used in this thesis are more hydrophobic than MeOH and relatively equally divided between the hydrophobic (octanol) and hydrophilic (water) phases. This would suggest the order of "[C_2mim][OAc] interaction": cellulose > water > EtOH >

[2] ¾ is the roughly estimated difference between CB and two AGUs, based on the different numbers of available OH groups in each (4 and 3).

[3] DMSO-CB (10 wt%) solution was mixed in various IL-DMSO mixtures, the heat of mixing was measured, and the heat of mixing of IL in pure DMSO was withdrawn. However, the $\Delta_{sol}H_{CB}$ in the DMSO that was dissipated when the DMSO-CB solution was prepared ahead of the experiment appears to have been neglected in that study. Perhaps it was assumed that it was of negligible size due to the very small effect measured for further dilution of 10 wt%-CB-DMSO solution in additional DMSO. In fact, $\Delta_{sol}H_{CB}$ in DMSO is ~ -20 kJ/mol(CB) (see 2.4.4) and should have been added to the calculation of $\Delta_{sol}H_{CB}$ in ILs, but was not. Thus, it is advisable to add $\Delta_{sol\ DMSO}H_{CB}$ (~ -20 kJ/mol CB) to the values in [57].

[4] The addition of 20 kJ/mol(CB) exothermal mixing enthalpy to the $\Delta_{sol}H_{CB}$s determined in [57 also changes to some curious endothermal values for known cellulose solvents, such as [$C_4C_1C_1$im][Cl], to exothermal.

2PrOH. However, when taking into account the confirmed strong H bonds to acetate (~100kJ/mol), the large $\Delta_{sol.\ [C2mim][OAc]}H_{water}$ (35 kJ/mol water compared to ~20kJ/mol AGU) and high HBD acidity of water, the actual order of water and cellulose must be inversed: water >> cellulose > EtOH > 2PrOH.[5]

2.4.3 DMSO - Nonsolvent & Cellulose

The interaction of nonsolvents and cellulose with DMSO is not as strong as their interaction with [C_2mim][OAc]. However, if a nonsolvent has less affinity for DMSO, it can increase the interactions with [C_2mim][OAc] and perhaps reduce the interactions of cellulose with [C_2mim][OAc] or increase cellulose-DMSO interaction.

$\Delta_{sol}H$ per mole of solute in pure DMSO for the solute compounds that are of interest to this thesis varies considerably: $\Delta_{sol}H_{water}$ = -5.4kJ/mol, $\Delta_{sol}H_{MeOH}$ = -1.4 kJ/mol, $\Delta_{sol}H_{EtOH}$ = 1.2 kJ/mol, and $\Delta_{sol}H_{1PrOH}$ = 2.6 kJ/mol[36]. Mixtures of DMSO with water and MeOH have been characterized in terms of H-bond acidity and basicity with solvatochromic probes[59]. The study found that acidity is drastically reduced from 1.06 (unitless scale in [59]), in pure water, to 0.16 at 60 mol% DMSO, thereafter the reduction is smaller, to 0.07 in pure DMSO. Most of the corresponding increase in basicity from 0.025 to 0.65 was found to be confined to the low range of DMSO concentrations. In MeOH, the basicity was found to be higher 0.55 and changed slowly with DMSO addition, whereas the acidity was only 0.4 and was reduced the most at very high DMSO concentrations, 80-100 mol%. The radical changes in H bond acidity and basicity over the range of water-DMSO mixtures are the consequence of strong DMSO-water interactions that leave only the dominant compound free to decide most of the solvation properties. In MeOH, the interaction is much weaker, which is why high acidity can be maintained even in 90 mol% DMSO. In consideration of the mixing enthalpies of the alcohols, EtOH and 2PrOH should interact with DMSO even less.

Exothermal swelling of cellulose in DMSO has been confirmed[60], which implies that DMSO interacts favorably with intercrystalline available surfaces. The mixing enthalpies of CB in water-DMSO mixtures (n_{water}:n_{DMSO}) have been measured [25]. Endothermal values of 9.7kJ/mol in pure water and of about 20kJ/mol in 80:20 mixture; isothermal mixing at 70:30; and exothermal values of -40kJ/mol in 33:67 and of -23kJ/mol at 5:95 mixture were found. Extrapolation from 33:67 through the 5:95 value gives the rough estimation of $\Delta_{sol}H_{CB}$ in pure DMSO at ~ -20 kJ/mol, which would imply $\Delta_{sol}H_{AGU} \approx$ -7.5 kJ/mol (½ of ¾ $\Delta_{sol}H_{CB}$) considering the differences between an AGU and CB. However, DMSO is not a solvent for cellulose, perhaps because of negative ΔS due to DMSO molecules tied to cellulose. The effect on entropy from such ties would be much smaller in cellobiose and increase with M_w.

Cellulose and water are likely to interact with DMSO, whereas the alcohols would have considerable selectivity for interactions with [C_2mim][OAc] in mixed solvents with DMSO.

[5] The *M*s of water and glucose are very different, which affects the entropy gain of mixing into the enthalpically unfavorable octanol phase. The high HBD acidity of water might exaggerate the high K_{OW} values of glucose in a way that is not relevant to the interactions with a HBA solvent.

2.4.4 Nonsolvent - Cellulose

The favorable or unfavorable interaction between nonsolvents and cellulose in solution affects the stability of ternary mixture with a solvent. For example a crucial difference between water and EtOH as the nonsolvent has been observed in molecular dynamics simulations of tetrabutylammonium acetate-DMSO cellulose solutions, which correlated with the stronger nonsolvent effect of EtOH [61].

Molecular dynamics modeling of cellulose oligomers in water and in MeOH have shown that both MeOH and water H bond to cellulose hydroxyl groups with about 20kJ/mol (bonds) as acceptors and with about 16kJ/mol (bonds) as donors[53]. This is in the same range as H bonds between neutral pairs of water molecules. However, the study found a difference in the numbers of H bonds. MeOH formed the same number of bonds as acceptor and as donor (1.3/AGU), whereas water formed about 1.7 bonds/AGU as acceptor and 2.3 as donor. The larger acidity and lower basicity of water, discussed in Subsection 2.3.4, would explain these relative numbers. However, the larger number of H bonds with water as acceptor compared to MeOH as HBA also indicates that water has an ability to fit in and form bonds where larger molecules would be hindered. In relation to cellulose, the very large sucrose solubility in water is interesting. It is almost two orders of magnitude larger than the solubility in MeOH, which is still about 10 times the solubility in EtOH [62]. Another related measurement is of the heats of wetting[60]. The heats of wetting are exothermal for water, several times more than for MeOH; roughly isothermal for EtOH; and increasingly endothermal for propanol and longer alkyl chains. However, the heats of wetting describe only the interaction with available intercrystalline surfaces. If a crystalline structure must be broken, such as the structure of CB, the mixing enthalpy in water is endothermal (9.7 kJ/mol CB [63]).

3 Materials and Methods

In this project, several methods were developed. For most of these new devices had to be constructed. Considerable time was spent building and rebuilding these prototypes. Here, however, only the ones that were used are briefly described. More detailed accounts are available in the Papers and in the Supporting Information of Paper II.

3.1 Materials

Two types of cellulose substrates were used in the study: microcrystalline cellulose (MCC) PH-101 (Mw=28.4 kDa, Mw/Mn=2.6, 97.2% glucan) and a hardwood kraft-dissolving pulp (Mw=162.3 kDa, Mw/Mn=3.1, 94.7% glucan). [C_2mim][OAc] was purchased from Sigma-Aldrich and was used as received (containing 0.5wt% H_2O, as determined by Karl-Fischer titration). Anhydrous DMSO was purchased from Sigma Aldrich and contained negligible amounts of water. Ethanol and 2-propanol (purities>99.5%) were purchased from Fischer Scientific.

3.2 Dissolution

MCC was added to the solvent and stirred with an overhead mixer turning a dough hook. The stirring speed was set at 800 RPM initially and then lowered to a level that did not cause the solution temperature to rise above 80 °C. A lid sealed the mixing vessel from the surrounding atmosphere so that no moisture could enter during stirring, which continued for two hours. The solutions were confirmed to be fully dissolved by verifying the absence of undissolved material between cross polarizing plates in microscope. Air trapped during stirring was removed from the solution by centrifugation before the solution was transferred to a syringe for moisture-free storage until use (within a week at room temperature).

3.3 CV Measurements

Coagulation values (CVs) were measured by monitoring the opacity of a thin film of cellulose solution, on a glass plate, while simultaneously following its weight gain due to nonsolvent vapors that it was exposed to. As a consequence of the absorption of the nonsolvent, the

solution precipitated and became opaque over a very short range of weight gain. The CV was then deduced from the plot of opacity versus weight uptake, as shown in Fig. 9, in terms of weight of nonsolvent added per initial weight of solution (in percent). The method was developed in-house as part of this project and involves numerous details regarding various issues, such as the control, minimization, and error estimation of moisture uptake from the air. Further details regarding these and other practical issues can be found in Paper I.

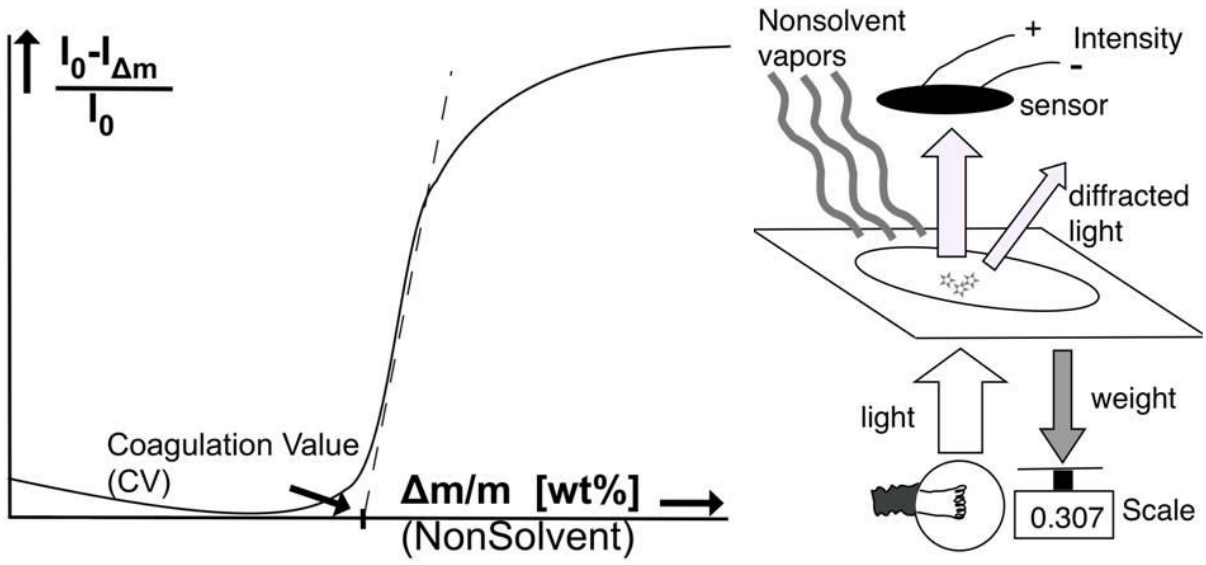

Figure 9. Left: opacity as a function of absorption of nonsolvent vapors into solution layer. CV indicated by sudden increase in opacity. **Right**: the setup used with the solution-coated glass slide translit and weighted simultaneously.

3.4 Mass Transport

For this method, we constructed a syringe-like device (see Fig. 10, Left) that could hold a well-defined volume of cellulose solution and then instantly extrude the whole solution. Prior to extrusion, the solution was well protected from surrounding moisture. After extrusion, it was shaped into a thin layer around an inert rod that was immersed in a nonsolvent. The solution was kept in the nonsolvent for a certain time. The weight of the syringe-like device with the solution attached was measured before and after immersion, which allowed for the calculation of the change in mass during immersion. The difference was normalized to the solution mass and termed Net Mass Gain, NMG. The NMG is equal to the sum of all mass transport to and from the coagulating solution. The mass transport of IL and DMSO was tracked using conductivity and NMR measurements of their respective concentrations in the nonsolvent bath. The mass transport of the only remaining compound, the nonsolvent, was obtained by combining the measurements of the NMG with those of the IL and DMSO, which diffused in the opposite direction. A full description can be found in Paper II.

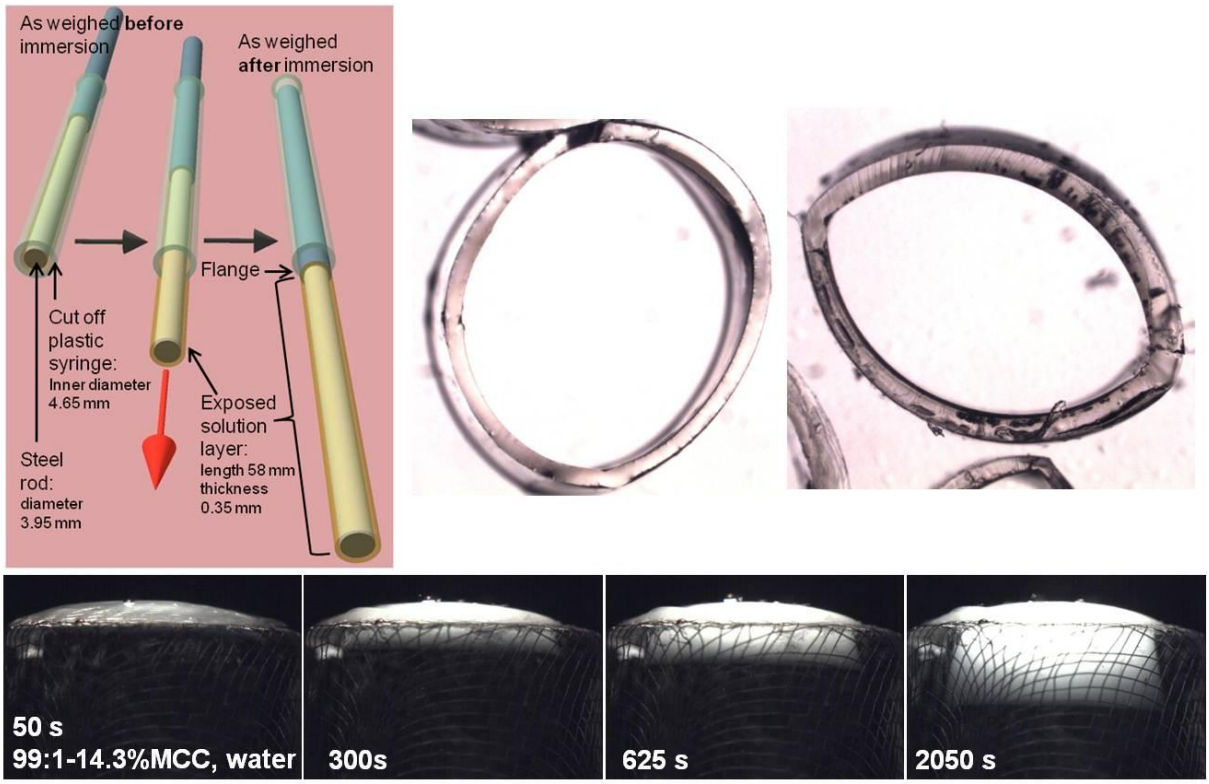

Figure 10. Left: a function of the device used for the mass transport measurements. **Right:** two sections of the membrane tubes (~5 mmwide) pulled from the rod after immersion in water for 10s and 45s (early method for coagulation rate measurements, later discarded). **Below:** the coagulation rate method used: 99:1-14.3wt% solution in a glass tube, the end of which was exposed to water. Images were taken after 50, 300, 625, and 2050s. The steel-wire net kept the swelling solution in place.

3.5 Coagulation Rate

To measure the propagation rate of coagulation, yet another method was developed. The method made use of a narrow glass tube, which was filled from one end with cellulose solution. The other end was sealed by inserting a glass rod. The solution was illuminated through the glass rod so that coagulation was observable as opaque regions. The tube was then placed vertically (solution exposed upwards) and observed from the side in microscope, as in Fig. 10, Below. The coagulation liquid level was raised above the open end, which initiated coagulation. The thickness of the coagulated opaque layer was measured and registered as a function of time. The data obtained displayed linear relations to the square root of time. The slopes of these linear relations supplied the rate coefficients evaluated.

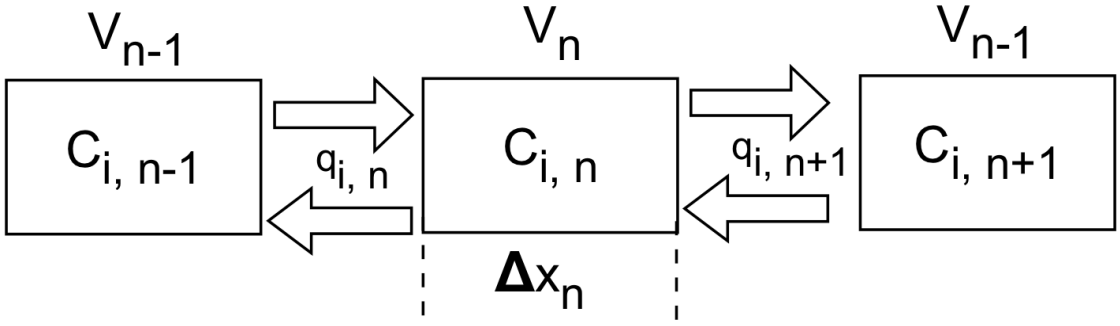

Figure 11. Neighboring volume elements (length Δx_n) of the numeric model $q_{i,n}$ are the fluxes and $C_{i,n}$ are the concentrations accumulated over time due to those fluxes.

3.6 Numerical Method for Modeling Diffusion

The diffusion observed in the measurements of mass transport and coagulation rate with water as nonsolvent were modeled by dividing the solution into volume elements (see Fig. 11) and calculating the concentration changes for 2-ms time steps with Eq. 9,

$$C(t + \Delta t)_n = C(t)_n + \Delta t \frac{D_n[C(t)_{n-1} - C(t)_n] + D_{n+1}[C(t)_{n+1} - C(t)_n]}{(\Delta x)^2} \quad (9)$$

where $D_n[C(t)_{n-1} - C(t)_n] = q_{i,n}$ and $D_{n+1}[C(t)_{n+1} - C(t)_n] = q_{i,n+1}$ are the sums of in- and outgoing fluxes through each of the surfaces to the left and to the right in Fig. 11, respectively. The $D_n(C)$s in Eq. 9 for the surface between each pair of two elements were calculated using the data for diffusivity of [C2mim][OAc] and water in [C2mim][OAc]-water mixtures, published by Hall et al. [37]. This is a simple finite difference model with few details added to it other than the basic diffusivity data. The purpose was to test a principle, not to replicate or predict data exactly.

3.7 Solvent Exchange

Coagulated samples from the mass transport measurements were saved for structural investigations. After storage in the same nonsolvent that was primarily used for the coagulation, a solvent exchange procedure was performed in order to preserve the originally coagulated structures for later investigations with SEM, XRD, and BET. Two solvent sequences were used: water→2PrOH→butanone→cyclohexane and 2PrOH→butanone→cyclohexane. The material was then dried from cyclohexane under dry N_2.

3.8 SEM

The material, was torn at room temperature to expose its fractured cross section, and then it was covered with 4 nm of Pt. This coverage was estimated based on the exposure time of the material in the sputtering device. The actual coverage of nanostructures, given their large porosity, must be significantly less. Images of specimen cross sections were then taken with a

Scanning Electron Microscope (SEM) from JEOL, model JSM-7800F, at 50k and 10k magnification.

3.9 XRD

The X-ray scattering was done at Lund University with a SAXSLab Ganesha 300XL instrument. This is a pinhole-collimated system for transmission mode. Data was collected with the detector placed at various sample-to-detector positions, which yielded an overall *q* range of $7.5 \cdot 10^{-2}$ – 2.6 $Å^{-1}$ for WAXS and $6.5 \cdot 10^{-3}$ – $1.8 \cdot 10^{-1}$ $Å^{-1}$ for SAXS. The dry isotropic samples were fixed perpendicular to the beam. The scattering pattern was recorded two-dimensionally and radially averaged. The mono-dimensional data thus obtained was deconvoluted into three crystalline and one amorphous peak over the *q*-range of 0.7 - 1.75 $Å^{-1}$. The "full width half peak heights" of those peaks were then entered into the Scherrer equation, which gives the crystallite dimension in each plane.

3.10 BET

The BET measurements of N_2 adsorption were performed on a Micrometrics TriStar 3000 Surface Area and Porosity Analyzer using a standard routine and 10 measurement points for adsorption and desorption in the pressure range of 0.01 – 0.15 atmospheres.

4 Results and Discussion

4.1 Phase Diagrams of Cellulose-Solvent-Nonsolvent Ternary Mixtures

4.1.1 Background

The properties of cellulose material precipitated from solutions depend on the composition of the solution prior to precipitation. Microscopic properties such as entanglement density, chain conformations, and relaxation behavior will depend on the amount of non-solvent present. Therefore, it is important to determine the degree of polymer nonsolvent dilution that precedes precipitation.

Phase diagrams for mixtures of 1-ethyl-3-methylimidazolium acetate ([C_2mim][OAc]), water, and cellulose have been investigated mainly by studying dissolution [48, 64]. These studies have shown very limited tolerances for water in the solvent. The dissolution process is known be complex and to depend on both properties of cellulose, e.g. M_w, microstructure and polymorph; and on parameters connected to the mixing, e.g. mixer type, shear rates, time and temperature. As IL-cellulose solutions often have rather high viscosities, there is a risk that thermodynamic equilibrium will not be reached within a finite dissolution time, due to slow mass transport. Solubilities measured with solid-state NMR by detecting cellulose-I, i.e. never-dissolved cellulose, in precipitated material are higher than solubilities measured with optical methods[64]. An interpretation of those results would be that although all the cellulose was penetrated and surrounded by solvent, it was never disentangled and dispersed. This is just one example of the multitude of parameters that make dissolution complex and that make the solubilities measured for dissolution different from solubility limits relevant to precipitation.

The available studies on the precipitation of cellulose that aim at determining critical concentrations for phase separation in IL-cellulose-nonsolvent systems are few, use only water as the nonsolvent, and are limited to relatively low and few cellulose concentrations.

Solubility limits have been measured with water as the nonsolvent for 0.5, 1, and 2wt% cellulose-butylmethylimidazolium chloride (C_4mimCl) solutions at 90-95°C [65] and for 1 and 9 wt% in [C_2mim][OAc], and 1wt% in two other ILs[66] .

Because most previous studies have looked at the limits of cellulose solubility only for dissolution, an investigation into the solubility limits for precipitation was an obvious first step in the project.

Table 2. CV values expressed in weight nonsolvent added per weight original solution. PH means that these solutions were preheated slightly (30-40°C), which was necessary in order to perform the measurement on these solutions. The solution designations: (wt% IL in solvent):(wt% DMSO in solvent) – (wt% cellulose dissolved) % (type of cellulose substrate), are used throughout this thesis.

	Solution composition			**H_2O**	**EtOH**	**2PrOH**
Solution designation	**MCC [wt%]**	**[C_2mim][OAc] [wt%]**	**DMSO [wt%]**	**CV [wt%]**	**CV [wt%]**	**CV [wt%]**
100:0-25%MCC (PH)	25.0	75.0	0.0	5.4	8.1	8.2
100:0-20%MCC (PH)	20.0	80.0	0.0	8.8	15.9	15.7
100:0-20%MCC	20.0	80.0	0.0	8.0	14.4	13.0
100:0-14.3%MCC	14.3	85.7	0.0	13.8	21.9	24.9
100:0-10%MCC	10.0	90.0	0.0	18.2	28.7	32.4
100:0-5%MCC	5.0	95.0	0.0	25.7	35.9	38.0
75:25-25%MCC (PH)	25.0	56.3	18.8	4.1	5.0	5.2
75:25-20%MCC	20.0	60.0	20.0	8.9	9.8	10.3
75:25-14.3%MCC	14.3	64.3	21.4	13.2	18.7	20.4
75:25-10%MCC	10.0	67.5	22.5	18.2	26.5	28.0
50:50-18.2%MCC	18.2	40.9	40.9	6.6	8.2	11.3
50:50-14.3%MCC	14.3	42.9	42.9	11.1	11.9	16.7
50:50-10%MCC	10.0	45.0	45.0	17.7	17.6	19.5
25:75-10%MCC	10.0	22.5	67.5	9.5	8.9	12.4
25:75-7.7%MCC	7.7	23.1	69.2	12.3	11.2	11.4
Dissolving Pulp (DP)						
100:0-14.3%DP	14.3	85.7	0.0	13.2	26.1	23.0
100:0-5%DP	5.0	95.0	0.0	23.8	41.1	40.2
50:50-14.3%DP	14.3	42.9	42.9	9.7	14.9	16.5
50:50-10%DP	10.0	45.0	45.0	15.6	18.1	19.7
25:75-7.7%DP	7.7	23.1	69.2	11.1	11.8	14.6

4.1.2 Different Nonsolvents

With a new method that was developed for this specific purpose, the data in Table 2 was obtained. The coagulation values (CVs) are the amounts of nonsolvent required to coagulate the solutions expressed in wt% of nonsolvent addition relative to the initial mass of solution.

However, the CVs in Table 2 are more easily interpreted if expressed in molar ratio (see Fig. 12), which shows that the nonsolvent tolerance is much reduced by high cellulose concentrations and solvent-DMSO contents. The CV_{mol} is also larger for water than for EtOH and 2PrOH (the lowest). The strong effects of high cellulose concentrations and high solvent-DMSO contents (lower [C_2mim][OAc] content) were expected results based on previous knowledge about H bond acceptors (Ac^-) and donors (cellulose and the nonsolvents), which interact strongly with each other. The question was how strong the effects were. The linearities observed in Fig. 8 are obvious and evaluating the slopes for each series enabled the observations of some finer details. The coefficients, *A* and *B*, in Eq. 10, where n_i signifies the molar concentrations, were fitted to the data and are summarized in Table 3.

Table 3. Parameters in Eq. 10 for the different solvent compositions and nonsolvent species, with the correlation coefficients (C.C.) for the resulting linear models. The last decimals have been kept because these were the evaluated parameters but only the first two digits are significant.

Solvent [wt:wt]									
[C_2mim][OAc]:DMSO	**A_{H2O}**	**B_{H2O}**	**C.C.**	**A_{EtOH}**	**B_{EtOH}**	**C.C.**	**A_{2PrOH}**	**B_{2PrOH}**	**C.C.**
100:0	2.349	0.367	0.99	2.226	0.630	1.00	2.336	0.742	0.97
75:25	1.808	0.284	0.99	1.901	0.503	0.98	1.907	0.613	0.97
50:50	1.592	0.172	0.99	1.418	0.469	0.94	1.149	0.574	0.43

$$n_{EmimAc} = A * n_{AGU} + B * n_{NS} \quad [10]$$

A and *B* are of significant interest because they supply measures for the balances between HBAs and HBDs, such as $A = n_{EmimAc}/n_{AGU}$ and $B = n_{EmimAc}/n_{NS}$. Taking Table 3 into consideration, it is apparent that *A* (for cellulose) is independent of the type of nonsolvent, although this statement is slightly less accurate for the 50:50-solvent composition. This observation supports the previous claim that A and B are measures of the interactions between specific HBAs and HBDs. It also motivates generalizing Eq. 11 into Eq. 11 with coefficients A-D in Table 4.

$$n_{EmimAc} = A * n_{AGU} + B * n_{water} + C * n_{EtOH} + D * n_{2PrOH} \quad [11]$$

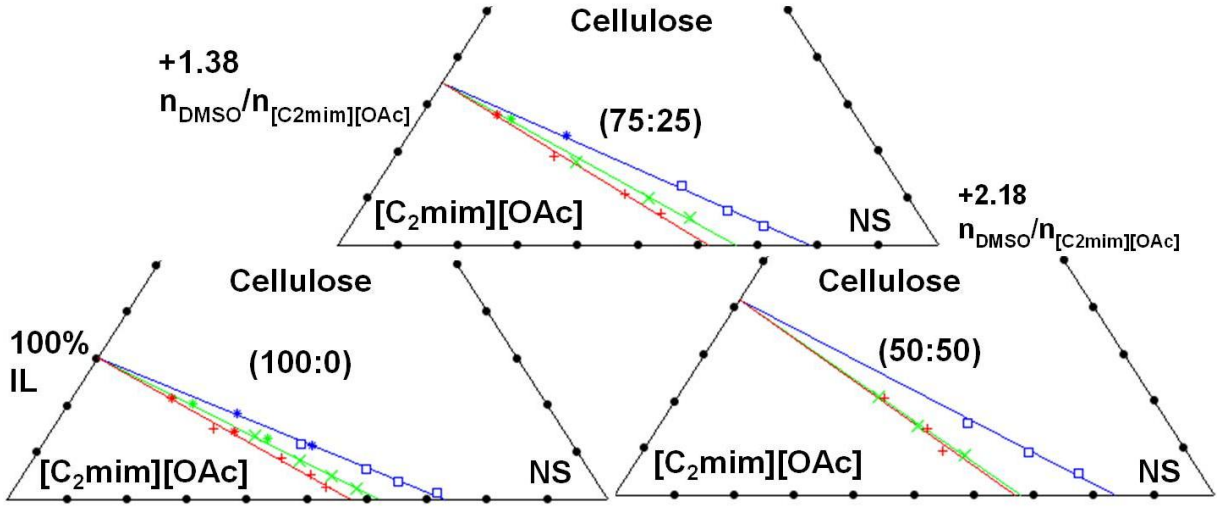

Figures 12. Ternary phase diagrams that describe the solubility limit in moles of AGUs, ([C_2mim][OAc] and nonsolvent (NS). The moles of DMSO were not included in the calculations of the molar ratios, as in Eq.10 and Eq. 11. The number of moles of DMSO that are also present in the solutions per mole [C_2mim][OAc] are indicated. Nonsolvent is either: water (blue), EtOH (green) or 2PrOH (red). Lines indicate the predictions of the linear models (the parameters in Table 4) that were based on the data. The points represent the measured data. The data points for the highest cellulose concentrations that required slight preheating are indicated by " * ".

Table 4. The parameters of Eq. 11 for different solvent compositions.

Solvent (wt:wt) [C_2mim][OAc]:DMSO	**A** $\frac{n_{EmimAc}}{n_{AGU}}$	**B** $\frac{n_{EmimAc}}{n_{H2O}}$	**C** $\frac{n_{EmimAc}}{n_{EtOH}}$	**D** $\frac{n_{EmimAc}}{n_{2PrOH}}$	**C.C.**
100:0	2.303	0.373	0.617	0.749	0.99
75:25	1.880	0.273	0.509	0.621	0.99
50:50	1.395	0.198	0.476	0.497	0.99

Various trends can be observed in these coefficients. *A* is reduced as an increasing amount of DMSO (0.72 and 2.17mol/mol) comes with every mole of [C_2mim][OAc]. This indicates a cellulose-solubilizing effect of DMSO, which can be explained by strong interactions between DMSO and cellulose. Both molecular dynamics simulations[61] and measurements, such as the mixing enthalpies of cellobiose in DMSO[63], have indicated an exothermal solvation of cellulose by DMSO. The values of $A_{100:0} = 2.3$ are of particular interest in relation to the 3 OH groups available on each AGU and the solubility limits for dissolution in pure [C_2mim][OAc] of about 2.5 n_{EmimAc}/n_{AGU} [48], because these values describe the minimum degrees of [OAc^-]-cellulose H bonding for precipitation and dissolution. Similarly $A_{50:50} = 1.4$ can be compared to the solubility limit of 1.5 n_{EmimAc}/n_{AGU} determined in a much more dilute [C_2mim][OAc] solvent [52]. The relative consistency between the different studies confirms that the majority of cellulose OH groups need to be H-bonded to acetate in order for the solution to be stable, but that DMSO can replace considerable amounts of these groups. The stronger coagulating effect of 2PrOH (>EtOH>H2O) is also reflected in *B*, *C*, and *D*,

which indicates that it takes about 2.7 water molecules to counteract the solvating effect of 1 [C_2mim][OAc] ion pair, but only 1.6 and 1.3 molecules of EtOH and 2PrOH, respectively, to have the same coagulating effect. The decreasing trends for $B, C, D = n_{EmimAc}/n_{NS}$ down the columns of Table 4 indicate attractive interactions between DMSO and nonsolvents . However, these trends, which imply a buffering effect of DMSO against the nonsolvent, were much stronger for water than for alcohols. This can be explained by the exothermal mixing measured for water and DMSO, which implies strong interactions between them. These effects of DMSO were later confirmed by molecular dynamics models in a similar acetate-based IL-DMSO system [61]. Fig. 13 shows the ratio of the CVs for the diluted solvents relative to the pure [C_2mim][OAc] solvent. The hatched lines indicate the levels that would be expected if DMSO was an "ideal" (passive) cosolvent. The difference between the "ideal" cosolvent level and the actual ratio can be considered as the solvation effect of DMSO in the solution.

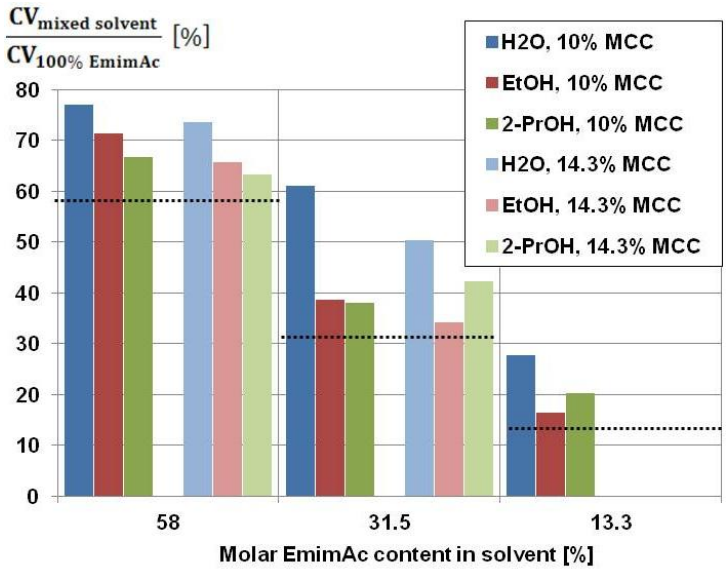

Figure 13. Ratios of CVs (wt%) for solutions in mixed solvents relative to the pure [C_2mim][OAc] solutions at equal cellulose concentration.

4.1.3 No Effect of Molecular Weight

There are numerous examples of molecular-weight dependence of cellulose dissolution. Therefore, a subset of the solution compositions was prepared with dissolving pulp (M_w=162kDa) instead of MCC (M_w=28.4kDa) to study the effect of M_w on coagulation. The whole data set from all 5 solutions and 3 different nonsolvents showed no significant general effect of M_w on the CVs . (see Table 2). This finding is not as surprising as it might seem, given that ΔS_{mixing} is relatively small for polymer dissolution, in most cases, and particularly small for cellulose due to its considerable stiffness. There are cellulose solvents, such as NaOH, that are temperature- and Mw-dependent[67] and, consequently, depend on ΔS_{mixing}. However, IL solvents have large exothermal mixing enthalpies with cellulose, which should make any differences in ΔS_{mixing} negligible in comparison.

4.1.4 Dissolution versus Precipitation (in Water)

Dissolution and precipitation processes depend on both thermodynamic (equilibrium) factors and kinetic factors. The equilibrium could be expected to be equal for both processes, but it is actually dependent on the free energies of the states prior to dissolution (generally crystalline cellulose I) and after precipitation (cellulose II of variable crystallinity). Kinetic factors, such as the diffusion of polymer segments, solvents, and nonsolvent, that are present during the dissolution and during the nucleation of new phases in precipitation are also likely reasons for differences between the two processes. A comparison between the results of this study and the results of previous studies on dissolution shows a large difference (see Fig. 14). There are variations in the dissolution data, which is expected given the known sensitivity of cellulose dissolution to the technique used. This indicates some degree of dynamic influence on dissolution. It has also been shown that solution viscosities start to change toward a gel-like state, at nonsolvent concentrations considerably lower than the CV [66]. The mobility of cellulose within a gel-like mixture is very low, which could further amplify the dynamic resistance to dissolution in this concentration range. However, the surprisingly low CV found by [66] for 1 wt% cellulose is also an indication that the solutions precipitated in our work could have been meta-stable over a considerable nonsolvent concentration range below the measured CV. Probably both of these dynamic phenomena combine to produce the difference, but it is not possible to distinguish and quantify their respective contributions to the total difference observed between dissolution and precipitation.

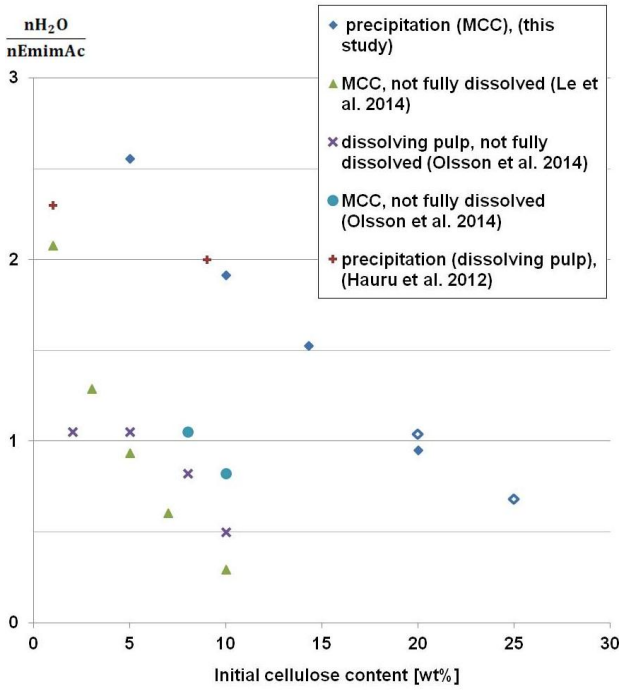

Figure 14. Comparison of dissolution and precipitation with regard to solubility of cellulose in $[C_2mim][OAc]$-H_2O mixtures, from different studies. **[48, 64, 66]**

4.1.5 Summary

- Mapping the phase diagram for the precipitation of [C_2mim][OAc]-Cellulose-(water/ EtOH/ 2PrOH) solutions provided a foundation for interpreting the results in the following sections.
- The coefficients of the linear relations that describe the solubility limits for precipitation provide a valuable measure for understanding effects between individual solvent species.
- The solvation of HBDs (cellulose and nonsolvent) by DMSO has an effect on equilibrium solubility. Previous studies on dissolution have interpreted the positive effects of DMSO as exclusively kinetic (lower diffusivity and viscosity), whereas the present study found that equilibrium solubility is also enhanced.
- The finding that Mw does not affect CV for the investigated range allowed the aspect of Mw in other investigations to be omitted and facilitated later work in the present study.
- The cellulose-[C_2mim][OAc]-water system displays strong inertia in its transitions from solid to solution and back to regenerated solid. The CV ranges of 4-26 wt% water, of 5-36 wt% EtOH, and of 5-38 wt% 2PrOH are significantly higher than the concentrations acceptable in cellulose dissolution.

4.2 Mass Transport during Coagulation

4.2.1 Background

In real-world industrial processes such as cellulose fiber spinning, the critical nonsolvent concentrations reported in the previous section do not come out of thin air, as the nonsolvent does in the method used in subsection 4.1. Molecules must move from the coagulation bath through the already coagulated parts into the still dissolved parts until the critical nonsolvent value has been surpassed. Because the nonsolvent is not supplied in the gas phase but by immersion, the solvent and cosolvent diffuse out of the solution at the same time.

Previous investigations have focused on the outward diffusion of solvent by measuring the concentration of solvent in coagulated shapes or in the coagulation liquids as a function of residence time in the coagulation liquid. Several studies have investigated both NMMO [68] [69] [70] [71] and ILs [72] [73] [71]. However, the coherence of the diffusion coefficients D_{IL} and D_{NMMO} that were reported in those studies varies because the mathematical models of diffusion used were, in many cases, erroneous. A few studies that are particularly confusing [68, 71], found initial (higher) and final (lower) apparent *D*s. In the first of these[68], an exponential expression was applied to a cylindrical geometry, whereas an infinite series of exponential functions of declining exponential coefficients would have been the proper expression[11]. Consequently, the multiple diffusion coefficients (exponential coefficients) that were found for short or long time scales can be expected as an artifact of incorrect mathematical treatment. In the second study[71], it is necessary to distinguish between the numerically modeled data and the experimental data. The numerical data is based on several,

unjustified assumptions regarding the effects of water and of coagulation on diffusion rates. In addition, the various coefficients that were evaluated for an arbitrarily chosen function varied by as much as ~30,000 times between different acetate-based ILs. The complexity of the model makes it difficult to follow exactly what was done and how the authors managed to confirm the erroneous multiple diffusion coefficients of their predecessors[68]. However, the experimental value, when evaluated conventionally, is consistent with several other studies [70] [69] [73, 74] that have made important contributions to the field. Unfortunately, there was an error in the first of these that was later replicated in the following studies. Equation 1 is the common equation used to calculate an apparent diffusion coefficient, *D*, for transient diffusion into an infinite slab based on the generally inexact but acceptable assumption that *D* is constant. The result is a kind of average value for *D* that is commonly termed "apparent" *D* and is very practical. However, there is a similar equation that applies to a membrane that is exposed from both sides[11]. This equation, which has a denominator of *4* instead of the *2* in Eq. 12, was used in those studies with the result that the values published underestimated *D* by a factor of *4*.

$$D = \left(\frac{M(t)}{M_{\mathrm{tot}}}\frac{d}{2}\right)^2 \frac{\pi}{t} \qquad (12)$$

The need to include the aspect of nonsolvent diffusion is particularly clear in the study of NMMO by Laity et al., [75] who used NMR imaging to show that the diffusion of NMMO through a cellulose solution gradually increases as a result of the initial infusion of water and the resulting phase separation. The CVs presented in Subsection4.1 were limited to a range of 5-30 wt %[76], which indicates that nonsolvent transport is the main contributor to and rate-controlling factor of phase separation.

A few attempts have been made to measure the diffusion of water into coagulating solutions of NMMO[70] and IL solutions[71]. However, the technique that has been used is an indirect one based on the observation of the coagulation-front propagation. That study assumes that the whole coagulated volume is composed of nonsolvent, i.e. that it is distributed as a step function with 100% NS in the coagulated part and 0% elsewhere. Discontinuous concentration profiles, such as a step function, are efficiently smoothed out by diffusive processes. Extraordinary circumstances would be required to maintain such a profile over time.

The actual nonsolvent distribution curves remain unknown for most cellulose solvent-nonsolvent combinations. To fill the knowledge gaps, which concern nonsolvent diffusion in particular, we developed a new method for the direct measurement of all diffusive fluxes. Complementary information was obtained from an enhanced version of the coagulation front method and numerical modeling as described in the Subsections 3.4-3.6. For more details, see Paper II and its supplementary information.

4.2.2 Evolution in Time

The progress of the coagulation process was followed through the mean concentration of each component and the change in total sample mass, which are shown in Fig. 15. These curves

were generated by repeated measurements for a wide set of different times. Each set of four data points in Fig. 15 corresponds to one measurement. The total mass relative to the initial mass, m/m_0 , illustrates the imbalance of flows: the initial dominance of inward nonsolvent diffusion (blue curve) over slower outward IL diffusion, by an increase up to a maximum, NMG_{max}, after ~100 s (for water in Fig. 15). At this point, the solution layer had coagulated throughout its thickness and a secondary process had begun. We chose to call the first stage "coagulation" and the second stage "washout." During the "wash-out" stage, IL diffused out and nonsolvent diffused in at relatively equal rates. The decline in mass during "washout" is the result of the lower density of the nonsolvent relative to the nonsolvent-IL mixture. This process was much slower and continued for ~10^3 s, compared to ~10^2 s for coagulation, in the 0.35 mm thick solution layers (for water, see Fig. 15).

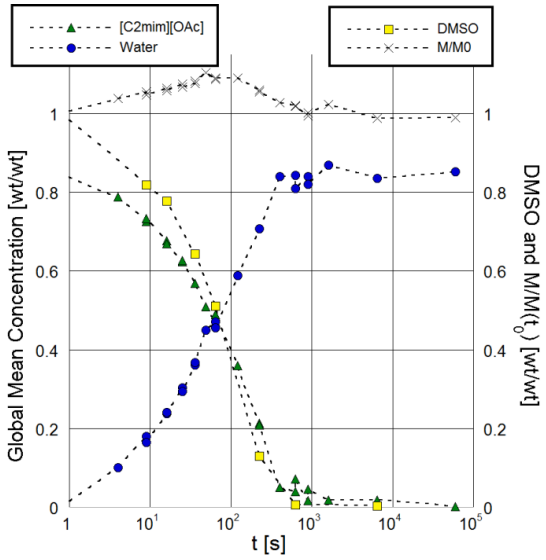

Figure 15. The mean-concentration developments in time for: [C_2mim][OAc], water, and DMSO (ratio relative to the initial concentration). The solution-mass ratio to the initial mass (crosses) is the sum of all flows. Lines are included to aid in connecting the curves with their theoretically known starting values.

In order to interpret these observations correctly, it is crucial to understand that the two stages or processes that we term "coagulation" and "washout," observed at different times before and after the observed maximum NMG, are really the progressions of "recently coagulated or coagulating" and "washed out" zones that were present at the same time but at different depths in the material. The data does not reflect the different local NMGs at different depths throughout the membrane. The data shows only a mean value of the different local NMGs, at any given time. Thus, at the end of ≈10^2 s, when the NMG maximum was observed, the first stage has dominated the process and its corresponding "coagulation" zone has penetrated the full membrane depth. Meanwhile, at that time, only a smaller fraction of the membrane depth has been affected by the washout stage. Figure 15 shows that after ≈10^3 s, the majority of mass loss has proceeded, which indicates that also the "washed out" zone has penetrated the full membrane depth. A useful characteristic of these transient diffusion processes is that the space variable, *x*, scales to the square root of time, as discussed in Subsection 2.2.3 [11]. This implies that the difference in time required for the advancing zones related to these stages to penetrate a certain depth may be translated into a difference in length scale. The ratio of the times for the two zones to reach full depth, which we

estimate to ≈10 times (i.e. $10^3/10^2$), yields a ratio of the penetration depths of the zones at the same time of ≈3 ($10^{1/2}$), as conceptually drawn in Fig. 16. The "coagulation" and "washout" stages are not envisaged as having distinct boundaries but, instead, as zones where one or the other process is dominant.

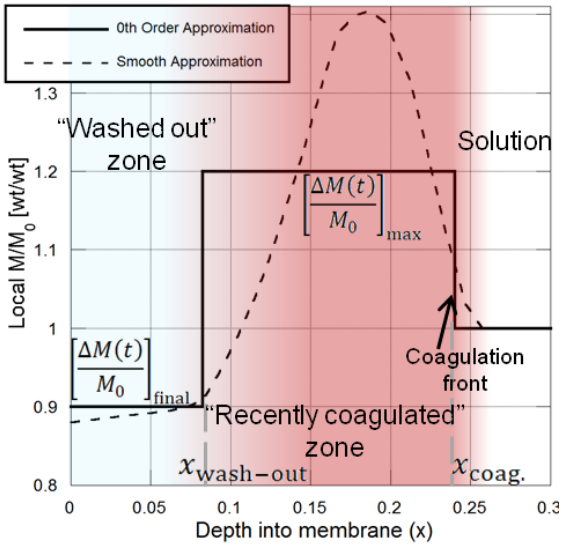

Figure 16. Illustration of how knowledge about the expanses of different zones relative to each other can be exploited to arrive at Eq. 13 and estimate a lower limit to the local NMG maximum. Net Mass Gain

Figure 17 shows curves for the NMGs as functions of time. Their maximum value is of interest because it corresponds to a local and temporary dilution of the polymer solution at a time that is critical to structure formation. Polymer concentration typically affects solution viscosity by a power ≈4 in concentrated cellulose-[C_2mim][OAc] solutions.[77, 78] Therefore, the NMG could have a significant effect on macromolecular dynamics during phase separation.

The NMG_{max} values increase in the order: 2PrOH > EtOH > H2O. They correlate approximately to the coagulation values, CVs, presented in Subsection 4.1. The CVs would provide a logical explanation for the variations in NMG_{max} because the [C_2mim][OAc] only becomes mobile after phase separation, which is incurred when the amount of nonsolvent prescribed by the CV has entered an incremental volume of the solution. Thereafter, the opposing diffusive volume fluxes of nonsolvent and [C_2mim][OAc] becomes more balanced. This makes the CV a central parameter for NMG_{max}. With 2PrOH as the nonsolvent, there is also a clear decreasing trend in NMG_{max} with increasing cellulose concentration. This too is consistent with CV dependence. However, the variations in NMG_{max} are much smaller than the corresponding variations in CV. There are also individual examples that contradict the correlation's generality, such as the comparison of 99:1-14.3%MCC coagulated in water (NMG_{max} ≈ 0.1 and CV=14 wt%) and 99:1-25%MCC in 2PrOH (NMG_{max} ≈ 0.15 and CV=8 wt%). NMG_{max} values are more dependent on the nonsolvent compound than on cellulose concentration. An explanation for this fact could be that more 2PrOH, than water, must be absorbed in the solution before an efficient washout of the [C_2mim][OAc] solvent can start. This would be due to the weaker affinity of [C_2mim][OAc] for 2PrOH (< EtOH < cellulose < water) and strong interactions with cellulose.

The measured NMG corresponds to an integral over the coagulated depth, and there are infinitely many distributions that all add up to the same mean. Consequently, knowledge about the local NMG maximum is quite limited when based only on the mass transport measured across the membrane surface, i.e. the value of the integral. However, knowledge about the level of NMG inside the "washed out" zone and about the expanse of the "washed out" zone restricts the way the total NMG can be distributed locally. Such restrictions can be exploited to quantify a lower limit of the local NMG maximum. The 0th order approximation in Fig. 16 exemplifies this principle, and from it follows Eq. 13 (derivation in SI of Paper II), which determines such a limit.

$$\left[\frac{\Delta M(t)}{M_0}\right]_{\max} = \left[\frac{\Delta M(t)}{M_0}\right]_{\text{tot}} \frac{x_{\text{coag.}}}{(x_{\text{coag.}} - x_{\text{wash-out}})} - \left[\frac{\Delta M(t)}{M_0}\right]_{\text{final}} \frac{x_{\text{wash-out}}}{(x_{\text{coag.}} - x_{\text{wash-out}})} \qquad (13)$$

The variables are marked in Fig. 16. Equation 13 sets lower limits to the NMG local maxima that are roughly 1.5 to 2 times the mean values observed. However, Eq. 13 assumes a discontinuous distribution, whereas the real distribution is necessarily continuous. This means that the real local peak value could be significantly greater than Eq. 13 suggests, as exemplified by the "Smooth Example" in Fig. 16. Thus, shortly after coagulation, the local degree of dilution is much greater than is shown in Fig.17. In certain cases, such as the 5wt% solutions and the 99:1-14.3%MCC solutions coagulated in alcohols, the local NMG maximum could be as high as 30-50%. Because these maximum local NMGs surpass the CVs of each solution, the volume expansions that correspond to these NMGs could be restrained by the coagulated structure. It can be assumed that a post-coagulation volume expansion corresponds to a stretching of the fibrils that hold the network together. However, in isotropic materials, the volume expansion associated with such local NMG would be divided on three dimensions. Therefore, as an example, a difference of 0.2 (20%) between the CV and the local NMG maximum, which corresponds to ~20% volume expansion after coagulation, would only imply ~6% elongation in each dimension ($\partial x = \partial V^{1/3}$). Consequently, the predicted post coagulation volume expansion appears reasonable.

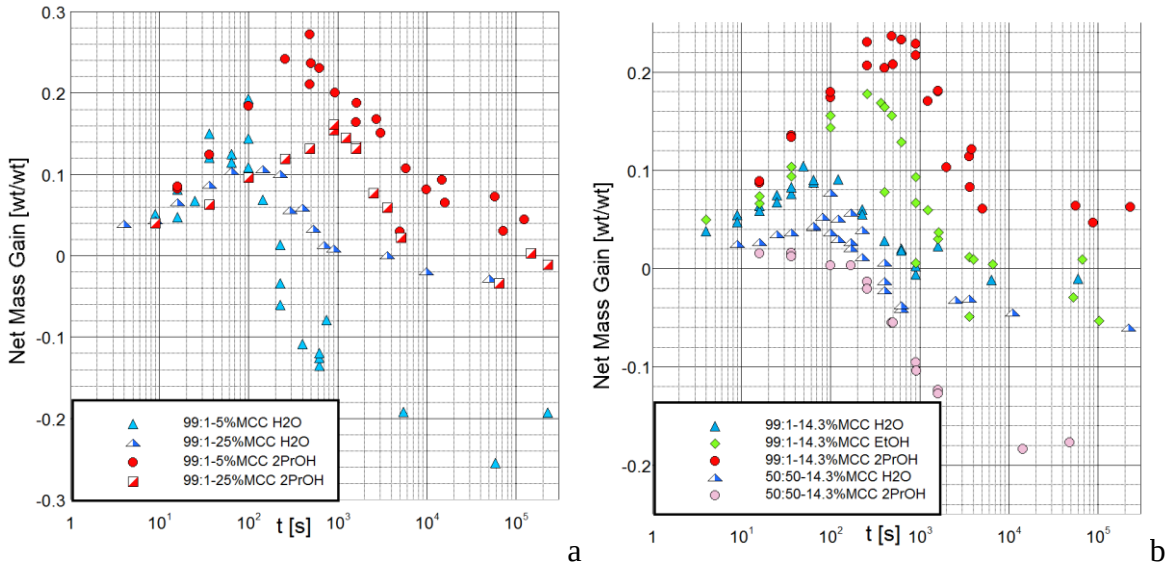

Figure 17. NMG as a function of time. The two stages of initial nonsolvent absorption during coagulation and secondary mass-loss during washout are displayed.

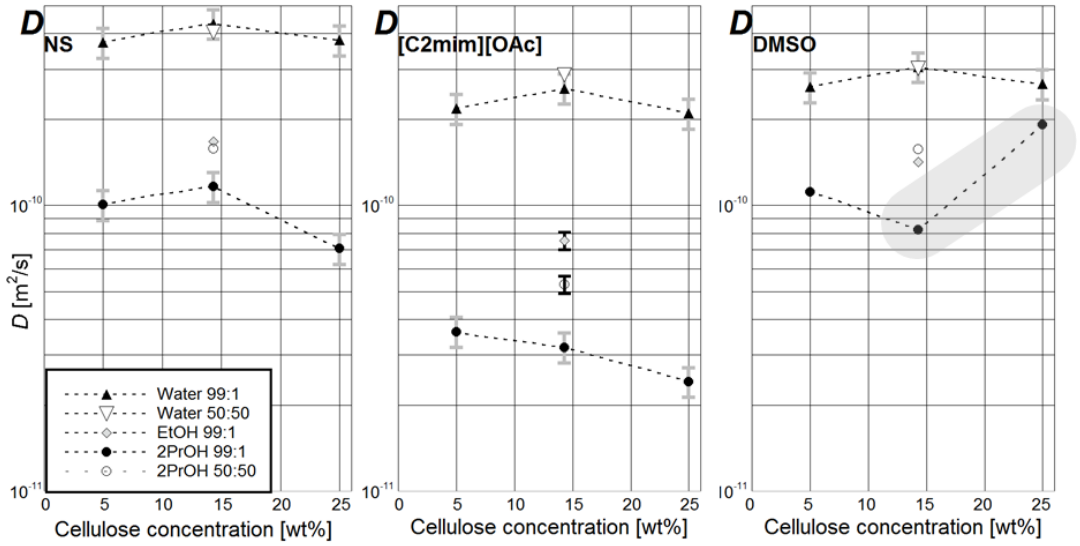

Figure 18. Apparent diffusion coefficients (D_{NS}, $D_{[\mathrm{C2mim}][\mathrm{OAc}]}$, and D_{DMSO}) during coagulation in water, EtOH or 2PrOH for: nonsolvent (**left**), [C_2mim][OAc] (**middle**), and DMSO (**right**). The shading serves to emphasize the uncertainty for some of the D_{DMSO} measurements.

4.2.3 Apparent Diffusion Coefficients

In Papers II and IV, the apparent diffusion coefficients, D_{NS}, $D_{[\mathrm{C2mim}][\mathrm{OAc}]}$, and D_{DMSO}, were measured and the results were as plotted in Fig. 18. All nonsolvents, except for 2PrOH, diffused faster than DMSO, which diffused faster than [C_2mim][OAc]. 2PrOH diffused at about the same rate as DMSO. The diffusion of all compounds was considerably faster with water than with the alcohols. However, the difference between coagulation in water and in alcohol was smaller for DMSO but significantly larger for [C_2mim][OAc]. The addition of DMSO increased diffusion significantly with 2PrOH as the nonsolvent, but with water, DMSO had only a marginal positive effect that was limited to $D_{[\mathrm{C2mim}][\mathrm{OAc}]}$. Even though the cellulose concentration was varied from 5 to 25 wt%, its effect was very limited, even insignificant with water as nonsolvent. Subsection 2.2 highlighted the effect of polymer in solution on small-molecule diffusion, but the diffusion of [C_2mim][OAc] in [C_2mim][OAc]-cellulose solutions is known to depend strongly on cellulose concentration[13, 14]. The fact that a large cellulose-concentration dependence was not observed for diffusion during coagulation, in our study, demanded an explanation. Figure 19 (Left)shows a comparison of the self-diffusion coefficients of [C_2mim][OAc][37, 79], water[37, 79], and DMSO[35, 79] in aqueous, in DMSO-, and in [C_2mim][OAc] solution to the mean of the apparent Ds during coagulation in water. These Ds from the coagulation experiments are about 5 times lower than the D_{self} s in aqueous solution, but as much as 20-40 times greater than the D_{self} s in [C_2mim][OAc]. In [C_2mim][OAc] solutions with 15 wt% dissolved cellulose, D_{self} of [C_2mim][OAc] is >200 times lower [13, 14] than the apparent $D_{[\mathrm{C2mim}][\mathrm{OAc}]}$ during coagulation. The conclusion from the high apparent *Ds* during coagulation, which were in the same order as the D_{self} s in the pure nonsolvents, and because a large effect from cellulose concentration was not observed was that coagulation forms a heterogeneous material with two co-continuous phases. Diffusion is conducted through the nonsolvent-rich phase, in which there is no cellulose present. In

that phase, diffusion proceeds just like in any liquid mixture of [C_2mim][OAc], DMSO, and a nonsolvent of the same concentration. This phase also constitutes the majority of the coagulated volume, at least with water as nonsolvent. Therefore, the cellulose does not affect the diffusion of [C_2mim][OAc], DMSO, or nonsolvent through coagulated parts, and a very minor part of the diffusion is conducted through parts that have not been coagulated.

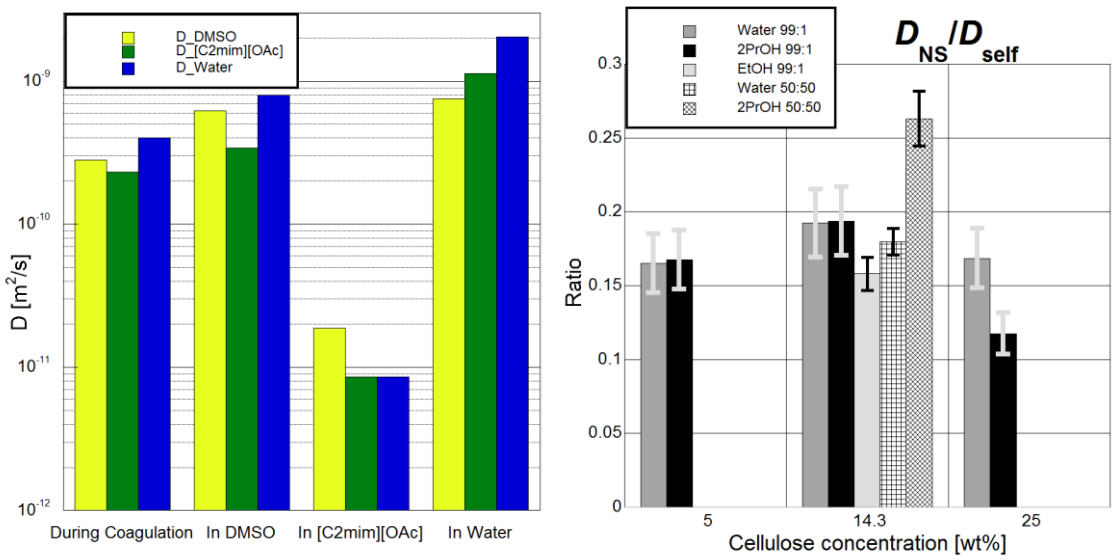

Figure 19. Left: Comparison of the mean apparent diffusion coefficients (the 99:1-[5, 14.3, 25]%MCC solutions coagulated in water), $D_{[\mathrm{C2mim][OAc]}}$, D_{Water}, and D_{DMSO} , with the diffusivities in each pure liquid. [35, 37, 79] **Right:** The ratios of the apparent diffusion coefficients, D_{NS}, to the self-diffusion coefficient [38, 80-82], of each nonsolvent.

4.2.4 Nonsolvent Diffusion

The apparent nonsolvent diffusion coefficients, D_{NS}, during coagulation correlated well with the respective self diffusivity, D_{self}, of each non-solvent. Figure 19 (Right) demonstrates this fact with a comparison of the ratios, D_{NS}/D_{self} , which are well-contained around the value $0.175 \pm 10\%$, except for the 50:50-14.3%MCC and 99:1-25%MCC solutions coagulated in 2PrOH. Based on the relatively general validity of this proportionality over a wide span of different conditions (C_{cell}, nonsolvents), it was concluded that D_{NS} depends mainly on the ability of the nonsolvent molecule to move through a liquid and the facility with which molecules travel through it. Strong interactions between specific pairs of solvent and nonsolvents, which could have inhibited or enhanced diffusion, appeared to have had a very limited effect. An exception could be the well-documented strong interaction between water and DMSO, which could explain why the D_{NS}/D_{self} for the 50:50-14.3%MCC solution was lower for water than for 2PrOH.

The coagulation front propagation rate coefficient, k_{coag}, describes the progressg of the phase-separated zone. Based on the values of k_{coag}, a "diffusion coefficient" can be calculated with Eq. 14.

$$D_{\mathrm{coag}} = \frac{\pi}{4}\left(k_{\mathrm{coag}}\right)^2 \tag{14}$$

From a mathematician's perspective, D_{coag}, actually describes the "diffusion" of coagulated volume if "coagulated volume" is hypothetically imagined to be a "substance." The ratio of the amount of non-solvent that has diffused in and the volume that the nonsolvent has coagulated quantifies how far into the material the nonsolvent has diffused. A certain amount of nonsolvent that has diffused in could either have spread evenly and induced coagulation very far into the solution with low concentrations throughout a large coagulated volume, or it could be confined to a very small coagulated volume, in which the nonsolvent concentration would be very high.

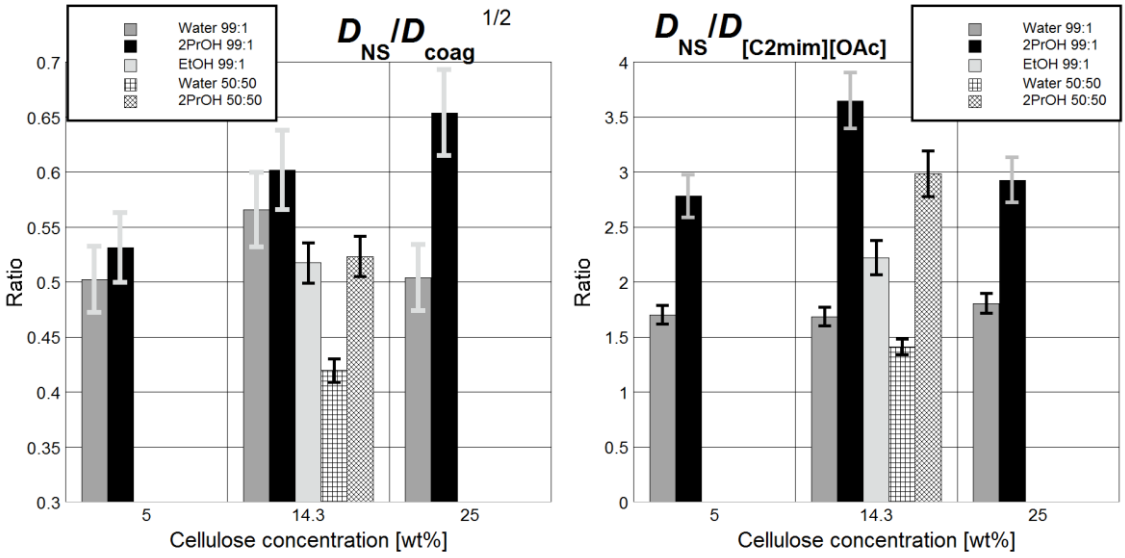

Figure 20. Comparison of different solutions and nonsolvents tested. **Left:** the ratios of the diffusion coefficient D_{NS} and D_{coag} (from Eq. 14). **Right:** The ratios of nonsolvent and [C_2mim][OAc] diffusion coefficients.

Figure 20 (Left) compares the concentrations of nonsolvent in the coagulated volume, which are expressed by the square roots of the ratios $D_{\mathrm{NS}}/D_{\mathrm{coag}}$. All values, but one, are above 0.5 (50%), which shows that the nonsolvent is generally concentrated to a rather limited coagulated volume. The nonsolvent concentration curves, thus, appear to be compact, probably with a steep decline through the coagulation front. Based on the trends in Fig. 20 (Left), these features would be more prominent for higher cellulose concentrations coagulated in 2PrOH, but less prominent with more DMSO in the solvent.

4.2.5 Effects of Cellulose on Diffusion

In Subsection 4.2.2, it was stated that cellulose does not affect diffusion very much. For some nonsolvents, this is a truth with modifications. With 2PrOH, the cellulose concentration actually has a limited but significant effect on several parameters, such as decreasing D_{NS}, $D_{[\mathrm{C2mim}][\mathrm{OAc}]}$ (see Fig. 18), and k_{coag} ; and the increasing ratio, $D_{\mathrm{NS}}/D_{\mathrm{coag}}$ in Fig. 20 (Left). Because a small amount of 2PrOH does not abstract the majority of [C_2mim][OAc] from the cellulose directly upon phase separation, such as a small amount of water would, it can be presumed that the volume fraction of diffusion-conducting nonsolvent phase is roughly proportional to the ratio C_{2PrOH}/C_{cell} during coagulation in 2PrOH. For 25 wt% cellulose solutions, which coagulate at a CV of 8wt% 2PrOH, this means that only about ¼ of the volume just behind the coagulation front is constituted by the 2PrOH-[C_2mim][OAc] phase. Only this limited volume fraction conducts the diffusion of 2PrOH to and [C_2mim][OAc] from the non-coagulated parts. The fact that the [C_2mim][OAc] in the cellulose phase is immobilized retards the diffusion of [C_2mim][OAc] even further, as shown in Fig. 20 (Right) by the ratios of $D_{\mathrm{NS}}/D_{[\mathrm{C2mim}][\mathrm{OAc}]}$ that are larger for 2PrOH. This effect is comparable to diffusion through a membrane with limiting diffusant solubility. The diffusant is transported from a volume (here, the cellulose-rich phase) with high solubility of the diffusant through a membrane (here, the 2PrOH phase) with low diffusant solubility, to another volume with high diffusant solubility (here the coagulation bath). The mass transport is reduced proportionally to the lower solubility in the conducting phase. The situation is slightly modified in the present study, in which solubility is replaced with an equilibrium [C_2mim][OAc] concentration in the nonsolvent phase. That concentration stands in equilibrium with the concentration in the cellulose phase. This equilibrium depends on the relative affinities of nonsolvent and cellulose for [C_2mim][OAc], and is similar to a nonsolvent-cellulose partition coefficient for [C_2mim][OAc]. Such "partition coefficients" are important to the diffusion during coagulation.

Another effect of cellulose is particular to the highest cellulose concentrations. At very high concentrations, the initial infusion of 2PrOH, which is needed to cause coagulation, becomes extremely slow. There are two reasons for this: the thermodynamic driving force for mixing is reduced due to less favorable [C_2mim][OAc]-2PrOH interactions and more unfavorable cellulose-2PrOH interactions when cellulose concentrations are high; and much slower diffusion of 2PrOH (bulkier than water) in the concentrated solutions. It was explained in Subsection 2.2 that diffusion in solutions is dramatically reduced when essentially all solvent molecules interact with the polymer, which is probably what happens at 25 wt% cellulose. This effect is, however, limited to the coagulation front and produces a local "barrier" to diffusion across the front. The "barrier" compacts the nonsolvent distribution curve and redistributes the nonsolvent concentration gradient from the whole coagulated parts to a smaller region around the coagulation front. The particularly reduced values of D_{NS}, D_{coag}, and $D_{\mathrm{NS}}/D_{[\mathrm{C2mim}][\mathrm{OAc}]}$ for 25 wt% cellulose in 2PrOH compared to 14.3 wt% are indications of this effect.

4.2.6 Numerical Model

The finding that coagulated material was heterogeneous and as such conducted diffusion in the same way as simple liquid mixtures do, implied that diffusion depends mainly on the [C_2mim][OAc] concentrations. Because the diffusivity data for that dependence in water had already been published [37], it was relatively straight-forward to produce an iterative numerical model for mass transport during coagulation.

The numerical model (see Subsection 3.6) models diffusion through a hypothetical porous solid medium that has 100% porosity and does not have any tortuousity but stops convection. Consequently, the numerical model represents only the liquid part of the coagulating cellulose. The model generated concentration curves for both water and [C_2mim][OAc], such as the curves displayed in Figure 21 for 1, 10, and 30 s. The model also predicts an NMG (water + [C_2mim][OAc]) and the coagulated depth based on where the water concentration exceeds the coagulation values from Paper I. The area under each curve for water, [C_2mim][OAc], and NMG can be evaluated by integration to obtain a model prediction of the total flux of each species. Figure 22 shows a comparison of the total fluxes of water and [C_2mim][OAc] (i.e. $M_{30}/M_{\infty \text{ or } 0}$).

The model predictions generally overestimate the mass transport observed in experiments to about the same degree for both compounds: 26-36% greater for water and 33-47% greater for [C_2mim][OAc]. The neglecting of tortuosity and other effects of cellulose on diffusion is a likely explanation for the moderate overestimation of mass transport rates. The NMGs in Figure 22 (Left) and coagulation depth after 30 s (see Fig. 22 Right) show good correlation between model and experiment, and the local NMG_{max} predicted is in excess of 1.25 times the initial density.

In summary, the relative success of the numerical model tested was another strong indication that the mass transport in these coagulating cellulose solutions can be described as liquid diffusion with only moderate errors incurred by neglecting cellulose. The model largely owes its success to the correct treatment of the strong dependence of such liquid diffusion on NS concentration.

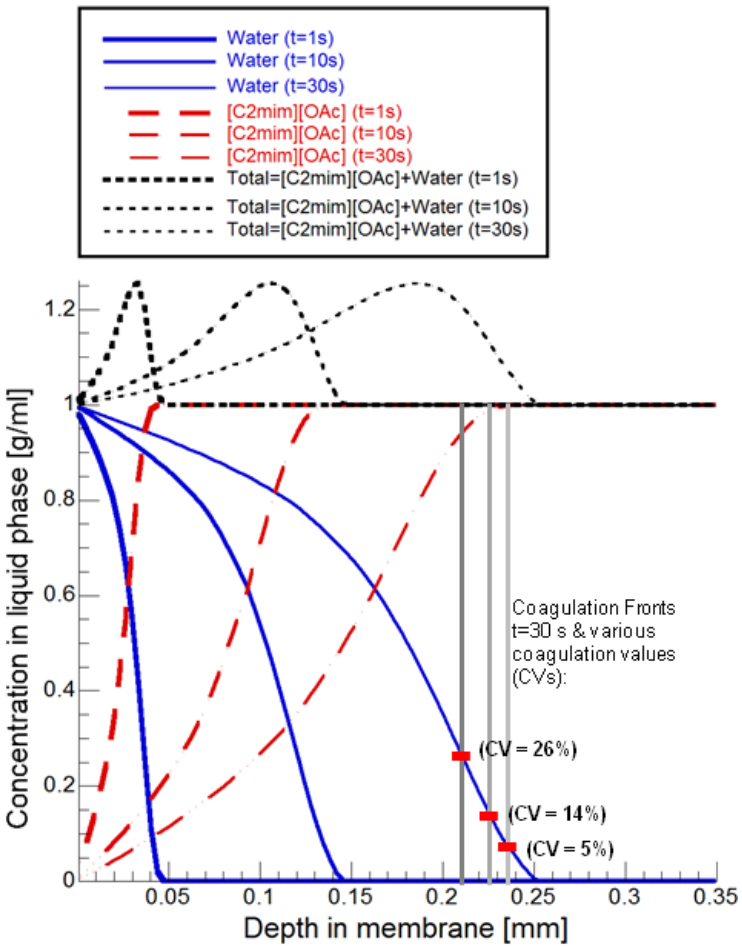

Figure 21. Model predictions for NMG (black) and the concentrations of [C_2mim][OAc] (red) and H_2O (blue) after 1s, 10s, and 30s, as a function of depth. The location of the coagulation front depends on the CV (grey bars).

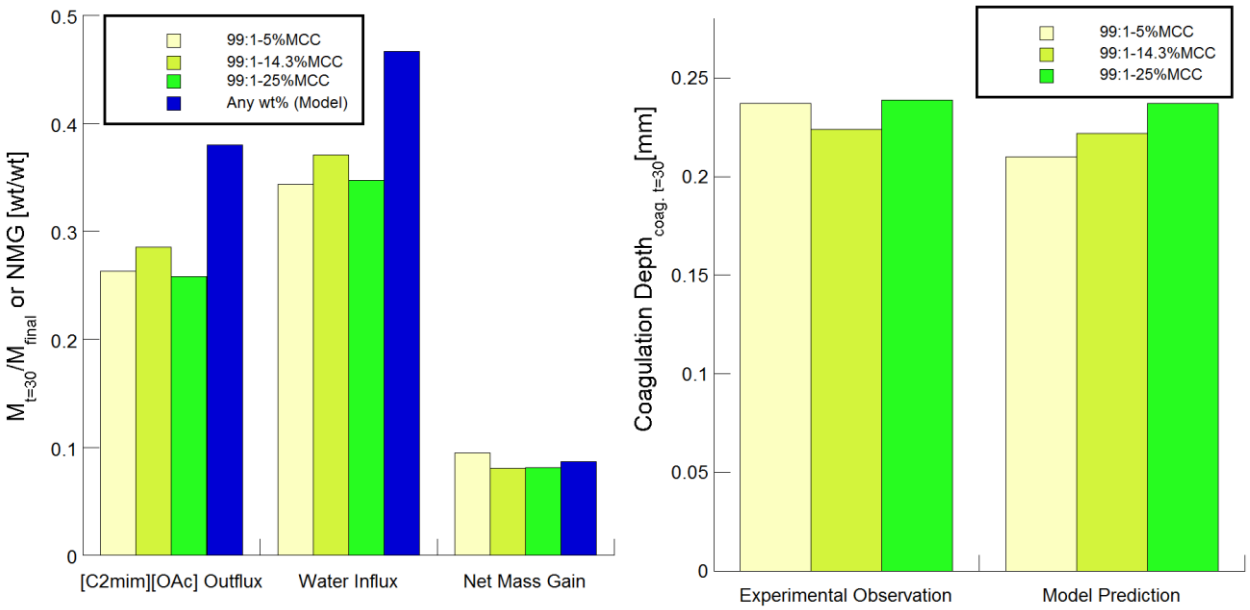

Figure 22. Comparisons of model and experiments (30 s): fluxes (**Left**) and coagulation depth (**Right**).

4.2.7 Summary

- The coagulation of [C_2mim][OAc]-cellulose solutions in water and 2PrOH is characterized by two stages: “coagulation” followed by “washout”, which propagate at different rates through the material.
- In the zone dominated by “coagulation,” the local NMG (dilution by nonsolvent) must be significantly larger than the global maximum NMG measured for the whole sample.
- The local maximum NMG is also larger than the CV, which indicates that a volume element continues to be diluted with nonsolvent also after it has been coagulated.
- The effect of cellulose on diffusion becomes marginal when it is restricted to a separate phase.
- The degree of separation can vary depending on the relative affinities of [C_2mim][OAc] for cellulose and the nonsolvent (water or 2PrOH).
- Water as nonsolvent represents a relatively ideal separation of cellulose from the [C_2mim][OAc] and nonsolvent, whereas 2PrOH gives a more complex situation with [C_2mim][OAc] interactions with both cellulose and nonsolvent.
- The simpler situation with water is very favorable for numerical modeling of coagulation.

4.3 Nanostructures, Crystalline Order, and Their Origin

4.3.1 Background

Most studies of cellulose structures precipitated from ILs have been performed with very specific applications in mind (cf. a recent review [83]). For this reason, a more general understanding of the effect of certain coagulation conditions on formed structures is lacking. Fiber spinning experiments have been performed using several different ILs, with air-gap [84-86] and conventional wet-spinning [87]. Most of these investigations have focused on the characterization of mechanical fiber properties, whereas the few microscopic properties tested have also been specific to fibers and their molecular orientation, such as birefringence and crystalline orientation. Where crystalline indexes (CIs) have been measured (WAXS or CP/MAS NMR), the results have been related to the anisotropicity of fibers. This means that much detail is lacking in understanding the kind of structures that are formed under given process conditions.

This section presents a study performed to better understand the formation of nanostructures during the coagulation of cellulose, for which mass transport was presented in Subsection 4.2. After coagulation and washing in the nonsolvent, solvent exchange was performed through a series of decreasingly polar solvents. The gently dried solvent-exchanged material was then characterized using BET measurements of specific surface area (SSA), WAXS, and SEM imaging. The structural changes usually induced by drying were avoided using this procedure, and structures originally coagulated could be studied.

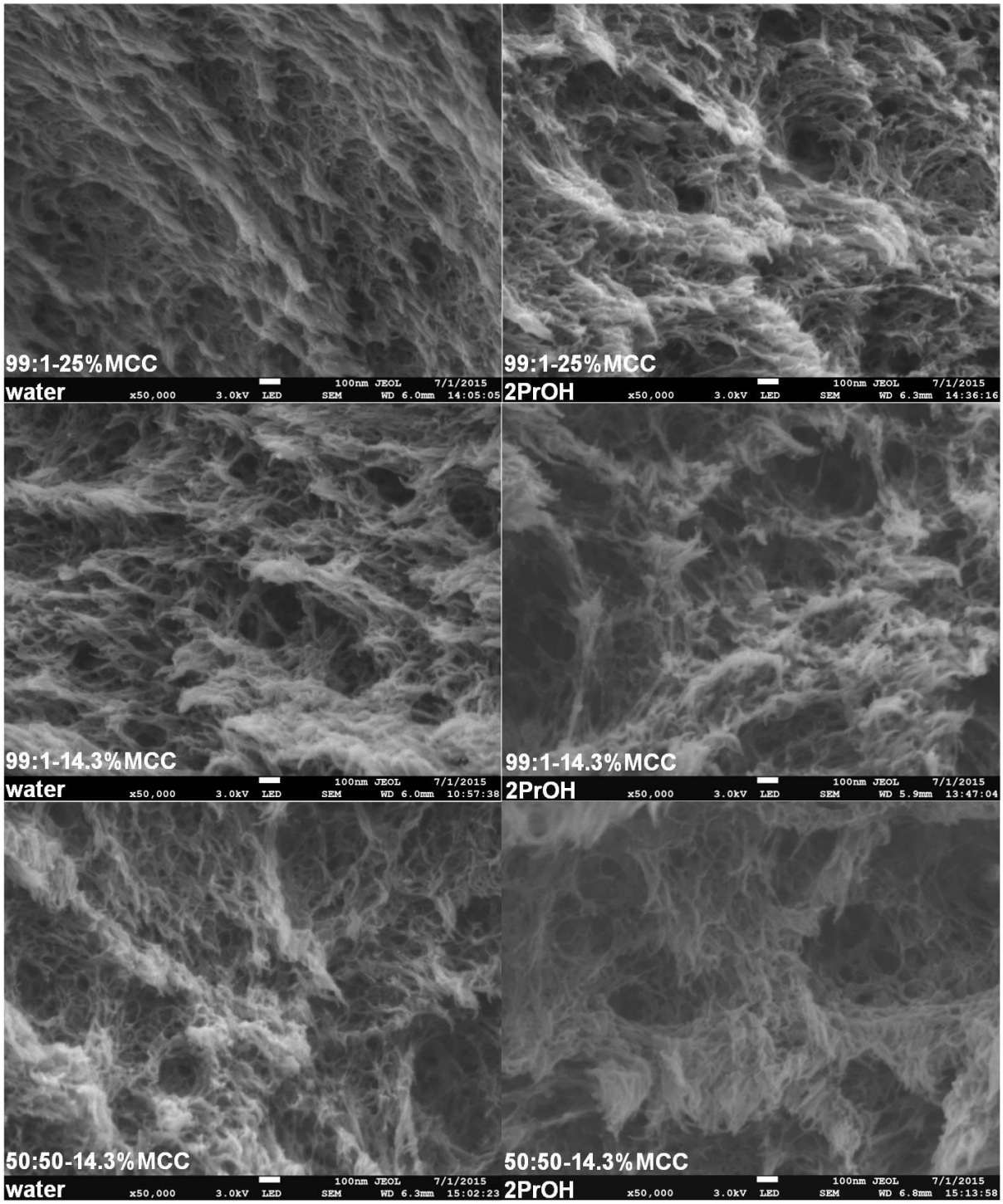

Figure 23. SEM images of solvent-exchanged dry materials at 50k magnification.

4.3.2 Nanostructuctural Build-up

Figure 23 shows the SEM images of these materials magnified 50k times. It can be seen that the cellulose fibrils have organized in open porous structures, which are even and contain many small pores of equal size when water was used as the nonsolvent. The networks are less homogenous if 2PrOH is the nonsolvent or with major DMSO dilution of the solvent. In these cases, large pores have formed, surrounded by denser regions with more fibrils and much smaller pores. The likeliest origin of the large pores is the liquid nonsolvent-[C_2mim][OAc] phase separated from a liquid cellulose-[C_2mim][OAc] phase during the primary phase separation. Based on the BET data, it was calculated that the fibrils were about 8-10 nm in diameter, assuming a round cross section, or about 5 nm thick, given a flattened ribbon-like cross section. The specific surface areas were larger, which means that the fibrils were thinner, following coagulation in water than in 2PrOH and for higher cellulose concentrations. However, as indicated by the diameter range of 8-10 nm, the differences were moderate. The investigations with WAXS (see Fig. 24) showed larger variations in terms of crystalline order and crystallite size. If coagulated in 2PrOH, the material showed significant observable order and stacking of cellulose chains, but only in one dimension (on the hydrophobic planes). Probably, most of the material had been organized only with regard to the closest neighboring chains, which produced a broad "amorphous" peak. In material coagulated in 2PrOH, the stacking of chains in the direction of the hydrophilic ($0\bar{1}1$) plane could be enhanced if later immersed and swollen in water. The enhanced stacking was detected through the appearance of the (020) peak (Fig. 24). When coagulated in water, the cellulose had much higher degrees of crystalline order and the crystallites reached significant sizes of up to about 7 by 3 nm, in the hydrophobic (011) and hydrophilic ($0\bar{1}1$) directions. This corresponds to about 15 by 4-5 cellulose molecules stacked in each direction perpendicular to the crystallite length. However, such crystallites constituted only part of the fibrils, which also contained a range of smaller crystallites probably down to what can be termed "amorphous." The WAXS spectra for material coagulated in water contained significant "amorphous" broad peaks, particularly with high cellulose concentrations. It was found that increased cellulose concentrations in water reduced crystalline order and crystallite sizes. The top row of Fig. 24 shows this fact clearly by the differences in sharpness of the spectra for 5, 14.3 and 25 wt% cellulose. 2PrOH yielded a constant low level of structural order for all cellulose concentrations. All the spectra of material coagulated in 2PrOH with different cellulose concentrations were identical to the center spectrum in Fig. 24. A radical difference was found between 2PrOH and water with regard to the smallest bits and pieces of the structures formed. In the next subsection, an explanation for how these differences is proposed.

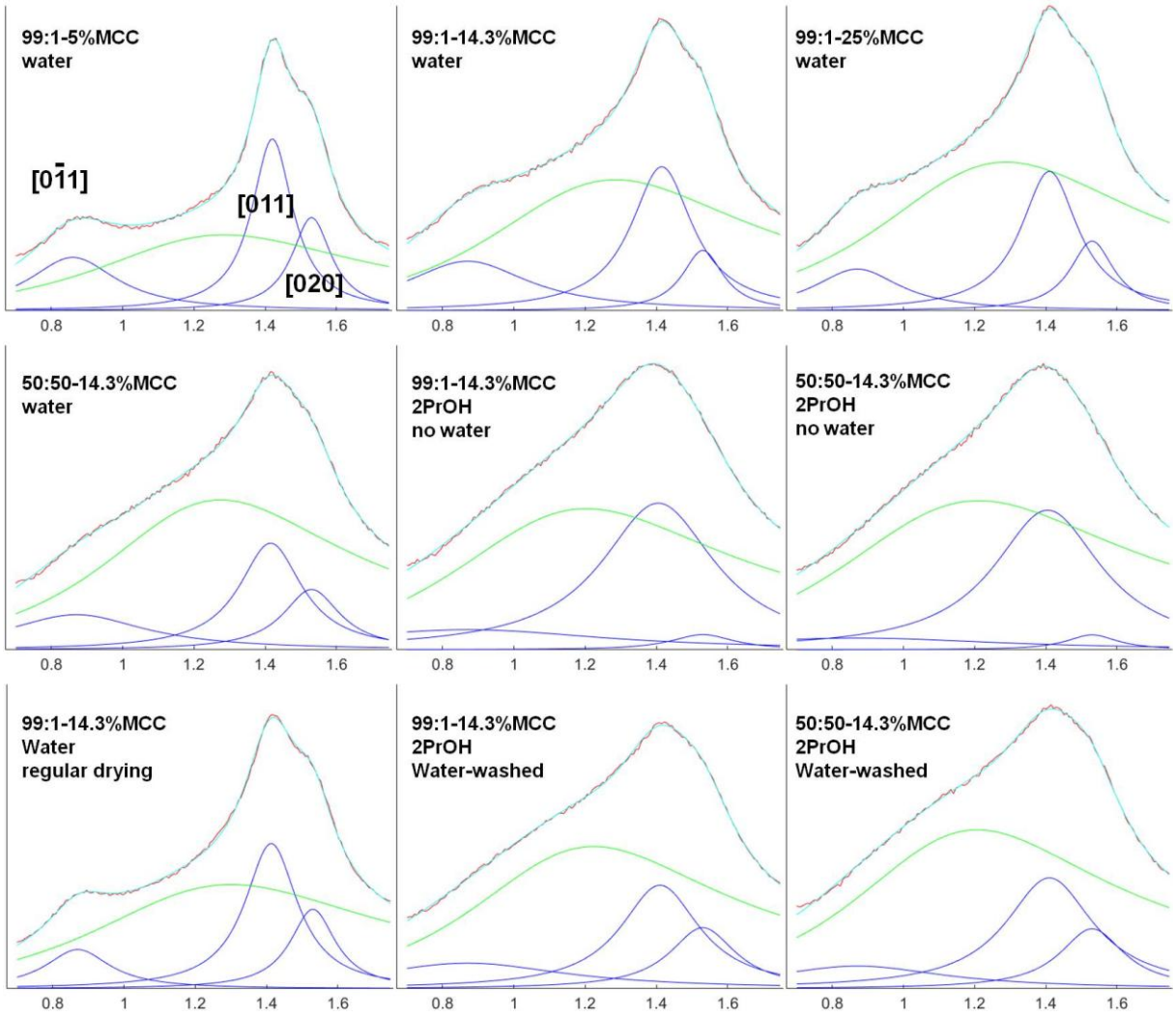

Figure 24. WAXS spectra with their respective deconvolutions (amorphous, green; crystalline, blue; model sum, cyan; data, red). Q-value in $Å^{-1}$ on the x-axis, linear intensity scale on the y-axis.

4.3.3 Nonsolvent Effects on Coagulation: Different Mechanisms

The extremely low crystalline order in materials regenerated in 2PrOH, or the reduction in crystalline order from DMSO in the solvent cannot be explained by the traditional explanations for varying degrees of crystallinity. For example, differences in cellulose mobility and the rate of phase separation are frequently attributed this role. Paper III presents an alternative explanation for these variations. In that paper, it is assumed that phase separation is a solid-liquid type with water as the coagulant and liquid-liquid with 2PrOH as coagulant, which, as stated in Subsection 4.3.2, is the likely origin of the large pores found in that material. Thus, two very different processes (see Fig. 25) will be described below.

Water diffuses into the solution interacting attractively with both [C_2mim][Oac] and cellulose (Fig. 25a). However, cellulose hydroxyl groups will gradually have less interaction with acetate anions and more with water. This makes the interaction with other cellulose-OH groups relatively more favorable and causes aggregation to start (see Fig. 25b). The figure shows that the cellulose chains are still well-solvated by the water-[C_2mim][Oac] mixture and even small crystallites are stable, which minimizes any free energy threshold to nucleation. It

can be speculated that the crystallites can reorganize slightly and grow under conditions of relatively high mobility. More cellulose in a solution means that less water is present, as shown by a lower CV, the concentration that incurs cellulose aggregation. Both the additional cellulose and the lesser amounts of water reduce the mobility of cellulose molecules during crystallization. This explains the lower crystalline order for high cellulose concentrations, which is similar to conventional theories on crystallization during cooling. After formation, the crystallites, which are interconnected by linking cellulose chains, adhere to the closest neighboring crystallites to the extent that the interconnections allow (Fig. 25c).

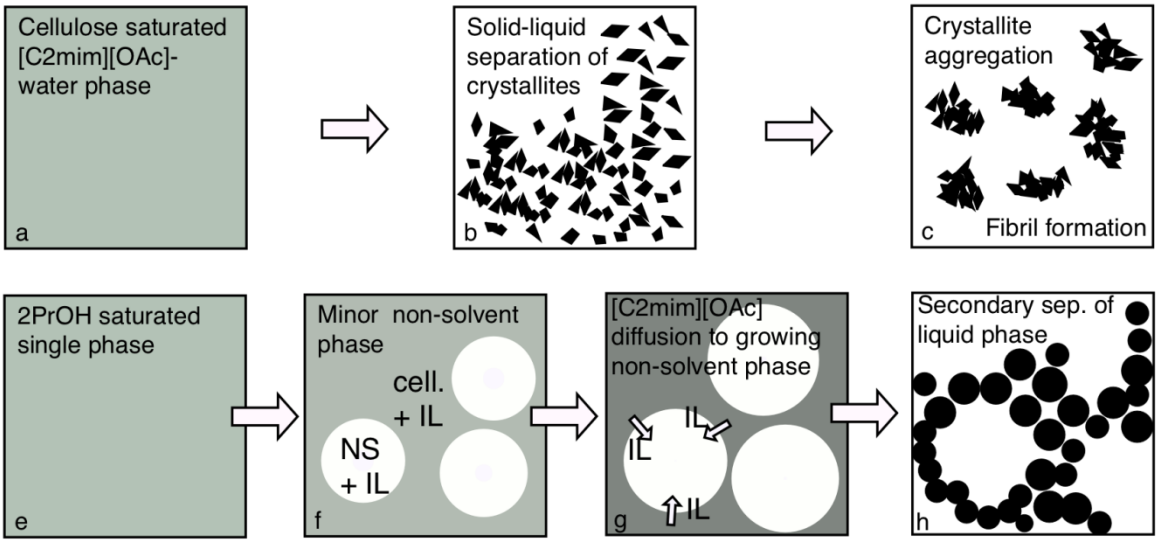

Figure 25. Schematic 2D cross sections of a volume undergoing phase separation and fibril formation by the different routes hypothesized. Water coagulation a-c: a) single-phase mixture of water, [C2mim][Oac] and cellulose; b) solid-liquid phase separation into solid cellulose crystallites (cross sections, black) and liquid [C2mim][Oac]-water phase (white); c) crystallites aggregated into fibrils. 2PrOH coagulation e-h: e) single-phase 2PrOH, [C2mim][Oac] and cellulose mixture; f) liquid-liquid-phase separation into liquid [C2mim][Oac]-cellulose major phase (grey) and liquid 2PrOH-[C2mim][Oac] minor phase droplets; g) gradual cellulose concentration increase as [C2mim][Oac] diffuses out; h) secondary phase separation of continuous phase into bicontinuous fibril network and [C2mim][Oac]-2PrOH phases.

2PrOH diffuses into the solution, where 2PrOH interacts attractively with [C_2mim][Oac] , but avoids cellulose (Fig 25.e). The consequence of this is that cellulose and 2PrOH interact with [C_2mim][Oac] as much as possible while avoiding each other. When the CV of 2PrOH has been reached, no cellulose crystallization occurs because it is more favorable to interact with [C_2mim][Oac] than to crystallize. Instead, a liquid cellulose-[C_2mim][Oac] phase is expulsed from, or expulses, a 2PrOH-[C_2mim][Oac] phase (Fig. 25f). The cellulose-rich phase gradually becomes more concentrated as more 2PrOH diffuses in to dilute the surrounding phase and abstracts more [C_2mim][Oac], which also diffuses out (Fig. 25g). At the concentration where cellulose finally starts to aggregate, the mobility of cellulose chains is very low. At that point, the concentration of cellulose could be higher than is possible to dissolve. The viscosity, which is essentially the inverse of cellulose mobility, is probably

close to infinite in such a solution. Consequently, the crystalline order is very low. The gradual depletion of [C_2mim][Oac] in the cellulose-rich phase also implies that the final structures are always formed from about the same cellulose phase of the same composition, independent of the cellulose concentration in the original solution. Based on the small pores that are present everywhere in the material coagulated in 2PrOH and visible with SEM (see Fig. 23), it appears that there is also a secondary formation of cellulose fibrils (Fig. 25h). These structures could be the result of some very inhibited “crystallization” process in the cellulose-rich phase.

This aspect of liquid-liquid and solid-liquid separation can also be described in thermodynamic terms. Figure 26. (Top) and (Bottom) shows hypothetical free-energy curves for mixtures of cellulose (right) and IL with nonsolvent (left). These curves reflect a likely scenario for the conditions of phase separation in IL solutions, based on the observations and background knowledge presented in this thesis. The solid black curves represent the pure IL solvent. A shaded zone represents the free energy of IL-cellulose mixtures for cellulose concentrations above the maximum solubility limit, in which the cellulose has started to aggregate and organize to varying extents. Close to the solid upper curve (amorphous liq. Limit), the mixture is completely amorphous and the cellulose-cellulose interactions are not at all optimized to cover for the reduction in IL interactions. Closer to the lower hatched line in the figure (crystalline limit), the cellulose is better organized with local crystalline structures surrounded by concentrated solution. The variation is continuous from the completely amorphous cellulose mixtures to the mixtures of perfectly organized cellulose and cellulose solution. The latter mixture will gradually resemble a two-phase system the closer it comes to the crystalline limit. With the addition of nonsolvent to the IL, the solid curve shifts as indicated by the red (2PrOH) or blue (water) hatched lines in the figures. The free energy is reduced in the IL-nonsolvent mixture, but it increases in the ternary mixture because of the lower affinity between nonsolvent and cellulose. The increase in free energy of the ternary mixture is particularly large for 2PrOH (Fig. 26 Bottom) and the reduction of the IL-nonsolvent mixture is more prominent for water (Fig. 26 Top).

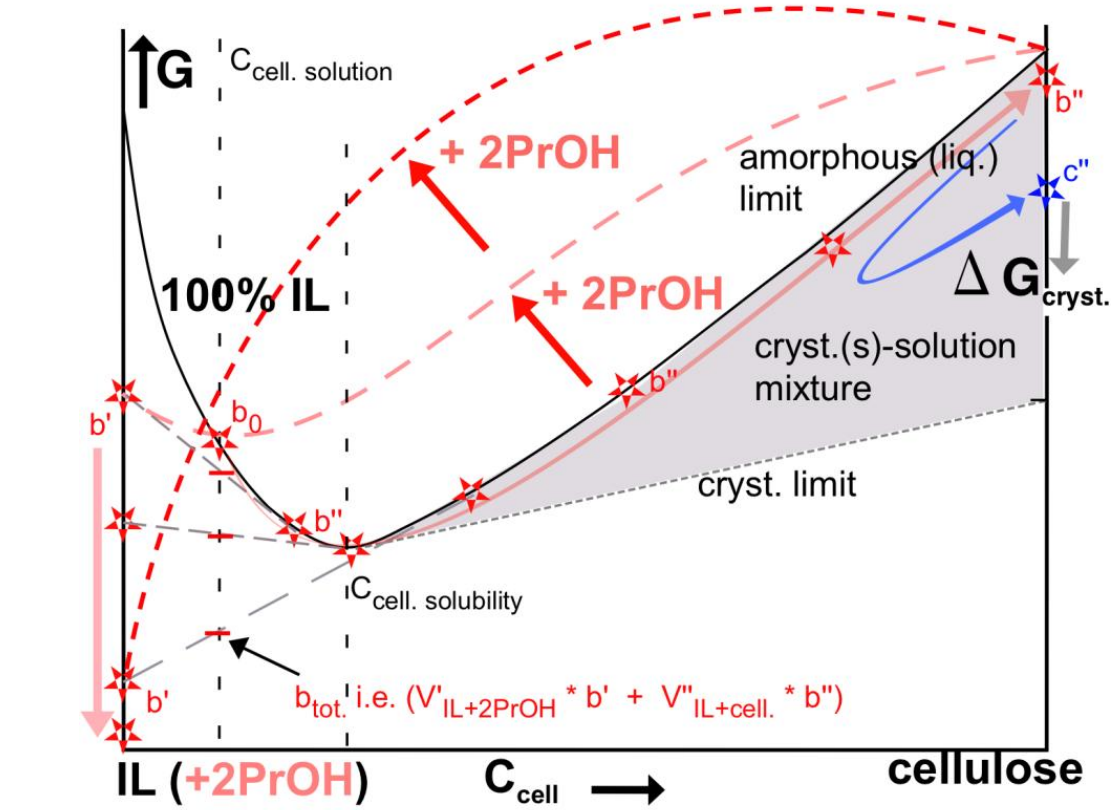
G
C cell. solution
+ 2PrOH
amorphous (liq.)
limit
b"
c"
100% IL
+ 2PrOH
Δ G cryst.
cryst.(s)-solution
mixture
b'
b0
b"
cryst. limit
C cell. solubility
b'
b tot. i.e. (V'IL+2PrOH * b' + V"IL+cell. * b")
IL (+2PrOH)
C cell
cellulose

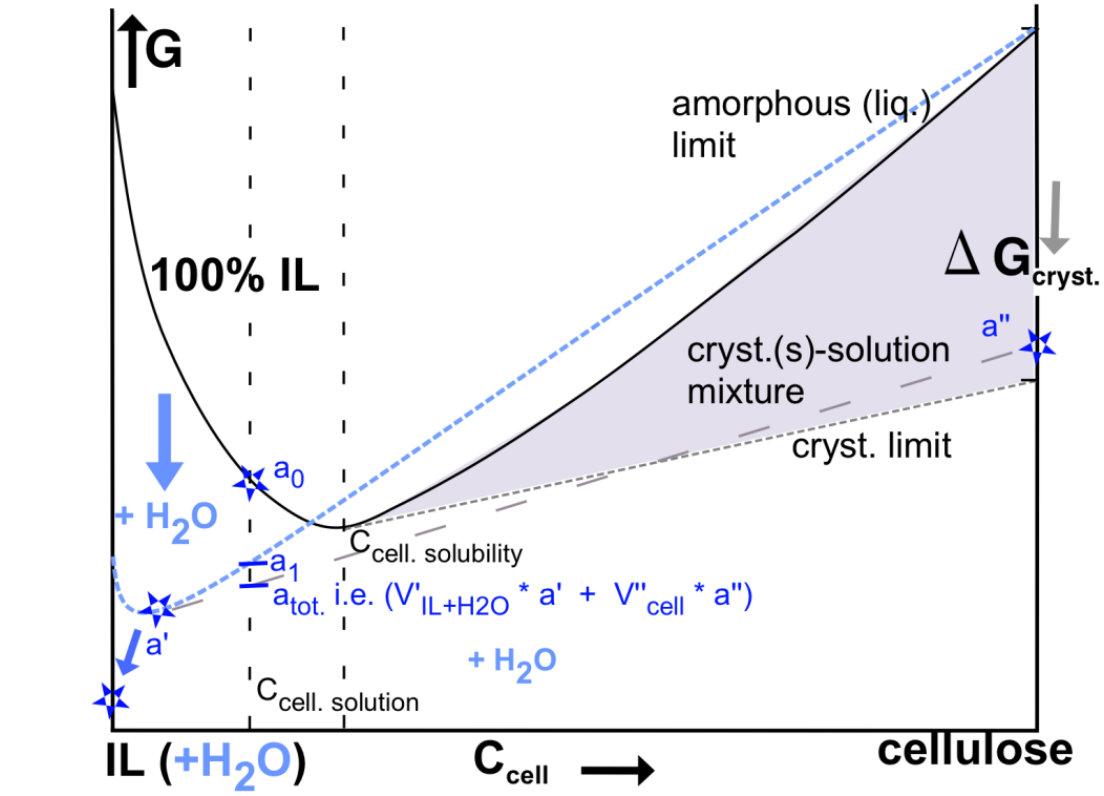
G
amorphous (liq.)
limit
100% IL
Δ G cryst.
a"
cryst.(s)-solution
mixture
cryst. limit
a0
+ H2O
C cell. solubility
a1
a tot. i.e. (V'IL+H2O * a' + V"cell * a")
a'
+ H2O
C cell. solution
IL (+H2O)
C cell
cellulose

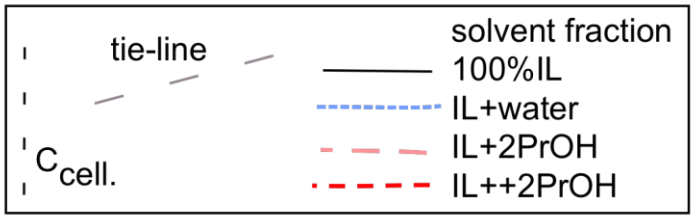
tie-line
C cell.
solvent fraction
100%IL
IL+water
IL+2PrOH
IL++2PrOH

Figure 26. Proposition for how coagulation works from a thermodynamic perspective. Schematic curves for the free energy, G, of mixtures of cellulose and IL (black solid), or IL- nonsolvent mixtures (water, blue; 2PrOH, red). Bars and stars indicate compositions. **Shaded zone**: beginning cellulose organization, mixture of saturated solution ($C_{cell.solubility}$) and very small cellulose domains, borderline single-dual phase. **Top**: Process with water solution at a_0, decrease in G to a_1 with increased water concentration, reduced total G by separation into *a'* and *a"* (crystalline), as the water concentration increases further G_{min} (and *a'*) continues to the left and all cellulose is crystallized at *a"*. **Bottom**: With 2PrOH, the G of the solution (intermediate $C_{cell.}$) at b_0 is initially little affected, G of the ternary mixture increases at higher concentrations, then G_{total} can be reduced by the formation of *b"* on the 100%-IL curve (solid black) and a *b'* of only IL and 2PrOH, *b'* and *b"* stand in equilibrium as *b'* reduces its G with increasing 2PrOH concentration and *b"* follows the 100%-IL curve toward $C_{cell.solubility}$. At $C_{cell.solubility}$, *b"* cannot crystallize efficiently for kinetic reasons and is forced up the 100%-IL curve to the right by the continuing reduction in the *G* of *b'* and the increase in volume of *b'*, with which *b"* stands in equilibrium. The final very poorly ordered *b"* can be swollen in water (blue arrow) and reorganizes to a more ordered, lower G, state *c"*.

Because water mainly reduces the free energy of the IL-nonsolvent side, cellulose remains in the ternary phase as the solution changes from a_0 to a_1 in Fig. 26 (top). However at a_1, it is favorable to form a crystalline phase *a"* from the IL-water-cellulose phase *a'* because this reduces the total free energy ($a_{tot.}$, on the tie-line between *a'* and *a"*). The crystallization of *a"*, which reduces the total enthalpy, can proceed in the ternary mixture because cellulose chains can move relatively freely there. The degree of crystalline order achieved depends on the amount of water present, which enhances the mobility of all molecules present, and on the concentration of cellulose chains present, which inhibit motion. The water-IL phase soon becomes void of cellulose and *a'* continues down the left vertical axis, as more water diffuses in.

Because 2PrOH addition increases the free energy of the ternary mixture, it becomes favorable to phase separate, in the first step, into one phase (*b"*) that remains on the black curve (Fig. 26, Bottom)for pure IL and one phase (*b'*) of IL-2PrOH. As more 2PrOH diffuses in and some IL diffuses out, the IL-2PrOH phase (*b'*) moves down the left vertical axis and the cellulose-rich phase (*b"*) moves along the black (pure IL-solvent) curve toward the cellulose solubility limit. At this point, crystallization becomes dynamically inhibited due to the low mobility of cellulose at high concentrations. Therefore, as phase *b"* continues to the right, it cannot crystallize and reduce the free energy. Consequently *b"* is restrained to the proximity of the "amorphous limit" until it reaches its final poorly organized state. *b"* appears to be so poorly organized that swelling in water gives it a slight fling into the shaded area before returning it in a slightly less disorganized state.

4.3.4 Summary

- Coagulated, but not yet dried, cellulose forms a network of fibrils the diameters of which are in the range of 8-10 nm if their cross sections are round.
- The fibrils are composed of crystallites, which can have cross-sections as large as 7 by 3 nm if coagulated in water. However, most crystallites are much smaller and some may not even count as proper crystallites.
- The organization of cellulose chains into crystallites is strongly inhibited if the cellulose is coagulated in 2PrOH. The organization is also largely limited to one crystalline plane.
- Individual larger pores are formed during coagulation in 2PrOH or when DMSO has been added to the solvent. Coagulation in water results in smaller pores of even sizes.
- The differences in structure formed with water and 2PrOH as nonsolvents are due to differences in the modes of phase separation with each nonsolvent. Water allows crystallization of cellulose from a ternary mixture. 2PrOH induces a separation of two liquid phases of which the cellulose-rich one later solidifies under conditions that limit macromolecular organizing.

5 Conclusions

In IL-cellulose solutions, water and alcohols share the same basic nonsolvent mechanism; they are H bond donors (HBD) in the place of cellulose OH groups, as previously known. The findings in Paper I confirmed this. However, water and alcohols are also very different nonsolvents, in particular, regarding how they interact with cellulose and how nonsolvents indirectly affect the interactions between cellulose and solvent. Water has the largest affinity for both cellulose and solvent (stronger than cellulose has), which makes it stronger in its fundamental HBD-nonsolvent mechanism, but this affinity also makes it act like a co-solvent toward cellulose. Alcohols are also strong HBDs, but the monohydric alcohols are weaker than both water and cellulose, which makes them rely more on large numbers of nonsolvent molecules and entropic effects to abstract the ionic-liquid solvent from cellulose. Nevertheless, their interactions with cellulose are quite unfavorable, as can be divined e.g. from the very low solubilities even of mono- and disaccharides in alcohols. This poor mutual affinity constitutes a secondary nonsolvent mechanism, which is not significant for water, and makes the total nonsolvent effect of alcohols stronger than the effect of water, as found in Paper I.

The differences in affinity toward cellulose and IL result in two distinctly different situations: one (water) in which all three components are relatively satisfied in the same phase; and the other (alcohol) in which two components (alcohol and cellulose) repel each other so much that they are separated into different phases once their concentrations are large enough. In the first case (water), the cellulose withdraws from the ternary mixture for the preference of interactions with itself that are favorable over, still attractive, interactions with the ternary mixture. In the second case (alcohols), the IL is attracted to both compounds and can maintain both compounds in a single phase for entropic reasons as long as the concentrations of alcohol and cellulose are low. However, at higher concentrations, the repelling compounds (alcohol and cellulose) encounter each other more frequently, which increases the mixture enthalpy. To avoid those encounters and reduce the solution enthalpy, the compounds separate into different phases, bringing as much IL as possible with them. The result is that cellulose maintains much more interaction with the solvent after phase separation in the latter case.

The structures formed by cellulose self-aggregation in solvent-nonsolvent (water) mixtures that have high cellulose affinities have relatively high degrees of crystalline order and large crystallite dimensions that increase with reduced cellulose concentration. The crystallites are assembled into nanofibrils that form an open porous network in which the pores are even in size. When two liquid phases are separated, one alcohol-IL and one cellulose-IL, the cellulose chains aggregate gradually as the IL is extracted from the cellulose phase. The presence of IL and the high cellulose concentration, in the cellulose-IL phase, disable the organizing of cellulose chains into regular crystalline structures. Consequently, the degree of crystalline order is low and the crystallite dimensions are small in the material formed. The initial liquid-liquid phase separation also leaves pores that are significantly larger than the small pores left between the fibrils formed from the liquid cellulose-IL phase when it is finally solidified.

The interaction between cellulose and solvent affects both the mass transport during the process and the cellulose structures formed by the process. Mass transport is mainly conducted through the nonsolvent liquid phase of the phase-separated parts of the coagulating solution. Cellulose-solvent interactions reduce the rates of mass transport across this coagulated part by means of several mechanisms:

- by reducing the volume that conducts the transport of ions and molecules
- by increasing the volume of the cellulose phase that is obstructive to mass-transport
- by retaining the IL ions and, thus, inhibiting their outward diffusion

If the concentration of cellulose is very high, the cellulose can inhibit the mass transport of certain nonsolvents into a non-separated single-phase solution. The reasons for this can be cellulose repellency of nonsolvents, preference for cellulose-IL interactions over nonsolvents-IL interactions, and inhibited diffusion.

In contrast, if the interaction between cellulose and solvent is small, the mass transport will be only slightly affected by the relatively isolated cellulose. This also makes the modeling of mass transport quite simple and straightforward.

That was the difference between water and alcohols as nonsolvents for cellulose-IL solutions.

This is the answer to a single very specific question that perhaps you did not ask. However, it emphasizes several aspects that are wider than this study and should be considered in future research on the shaping of cellulose with ILs and other aprotic solvents. Looking into these aspects will increase the chance of finding new processes for renewable production of cellulose fibers.

6 Acknowledgements

This research was funded by ‘Södra Skogsägarnas stiftelse för forskning, utveckling och utbildning’.

I have also enjoyed the support of senior colleagues at Swerea IVF AB, where I am employed. Without their patience, and prioritizing of the rather fundamental research that was presented in the above, the project might not have come to this point.

I would also like to thank the following people for their support during this time:

- My advisors and constant co-authors Tobias Köhnke and Hans Theliander
- Everyone within the Avancell project
- My colleagues at Swerea IVF and at Chalmers University of Technology (especially those who have helped me to adapt to the local bureaucracy)
- Friends and family

7 References

1. The_Fiber_Year_GmbH, *The Fiber Year (2017) World survey on textiles & nonwovens*, A.W. Engelhardt, Editor. 2017: Speicher, Switzerland.

2. Woodings, C., *Regenerated cellulose fibres*. Vol. 18. 2001: Woodhead Publishing.

3. Swatloski, R.P., et al., *Dissolution of cellose with ionic liquids.* Journal of the American Chemical Society, 2002. **124**(18): p. 4974-4975.

4. Hermanutz, F., et al. *New developments in dissolving and processing of cellulose in ionic liquids*. in *Macromolecular Symposia*. 2008: Wiley Online Library.

5. Strobl, G.R., and SpringerLink (e-book collection), *The Physics of Polymers: Concepts for Understanding their Structures and Behavior*. . 2007, Berlin: Springer, New York.

6. Jones, R.A., *Soft condensed matter*. Vol. 6. 2002: Oxford University Press.

7. Van de Witte, P., et al., *Phase separation processes in polymer solutions in relation to membrane formation.* Journal of Membrane Science, 1996. **117**(1-2): p. 1-31.

8. Witte, P.v.d., et al., *Metastable liquid-liquid and solid-liquid phase boundaries in polymer-solvent-nonsolvent systems.* Journal of Polymer Science, Part B: Polymer Physics, 1997. **35**(5): p. 763-770.

9. Fick, A., *V. On liquid diffusion.* The London, Edinburgh, and Dublin Philosophical Magazine and Journal of Science, 1855. **10**(63): p. 30-39.

10. Cussler, E.L., *Diffusion: mass transfer in fluid systems*. 2009: Cambridge university press.

11. Crank, J., *The mathematics of diffusion*. 1979: Oxford university press.

12. Phillies, G.D., *Phenomenology of polymer solution dynamics*. 2011: Cambridge University Press.

13. Ries, M.E., et al., *Diffusion of 1-ethyl-3-methyl-imidazolium acetate in glucose, cellobiose, and cellulose solutions.* Biomacromolecules, 2014. **15**(2): p. 609-617.

14. Lovell, C.S., et al., *Influence of cellulose on ion diffusivity in 1-ethyl-3-methyl-imidazolium acetate cellulose solutions.* Biomacromolecules, 2010. **11**(11): p. 2927-2935.

15. Gavillon, R. and T. Budtova, *aerocellulose: new highly porous cellulose prepared from cellulose- NaOH aqueous solutions.* Biomacromolecules, 2007. **9**(1): p. 269-277.

16. Muhr, A.H. and J.M. Blanshard, *Diffusion in gels.* Polymer, 1982. **23**(7): p. 1012-1026.

17. Kraessig, H., et al., *Ullmann's Encyclopedia of Industrial Chemistry*. 2002.

18. Kondo, T., *The relationship between intramolecular hydrogen bonds and certain physical properties of regioselectively substituted cellulose derivatives.* Journal of Polymer Science Part B: Polymer Physics, 1997. **35**(4): p. 717-723.

19. Haines, A.H., *Relative reactivities of hydroxyl groups in carbohydrates*, in *Advances in Carbohydrate Chemistry and Biochemistry*. 1976, Elsevier. p. 11-109.

20. Feng, S., C. Bagia, and G. Mpourmpakis, *Determination of proton affinities and acidity constants of sugars.* The Journal of Physical Chemistry A, 2013. **117**(24): p. 5211-5219.

21. Moon, R.J., et al., *Cellulose nanomaterials review: structure, properties and nanocomposites.* Chemical Society Reviews, 2011. **40**(7): p. 3941-3994.

22. French, A.D., *Idealized powder diffraction patterns for cellulose polymorphs.* Cellulose, 2014. **21**(2): p. 885-896.

23. Langan, P., Y. Nishiyama, and H. Chanzy, *A revised structure and hydrogen-bonding system in cellulose II from a neutron fiber diffraction analysis.* Journal of the American Chemical Society, 1999. **121**(43): p. 9940-9946.

24. Medronho, B., et al., *Rationalizing cellulose (in) solubility: reviewing basic physicochemical aspects and role of hydrophobic interactions.* Cellulose, 2012. **19**(3): p. 581-587.

25. Bergenstråhle, M., et al., *Simulation studies of the insolubility of cellulose.* Carbohydrate Research, 2010. **345**(14): p. 2060-2066.

26. Segal, L., et al., *An empirical method for estimating the degree of crystallinity of native cellulose using the X-ray diffractometer.* Textile Research Journal, 1959. **29**(10): p. 786-794.

27. Liebert, T., *Cellulose solvents: remarkable history, bright future*, in *Cellulose solvents: for analysis, shaping and chemical modification*. 2010, ACS Publications. p. 3-54.

28. CrcnetBase, *CRC handbook of chemistry and physics*, Cleveland, Ohio: CRC Press.

29. Ballinger, P. and F. Long, *Acid Ionization Constants of Alcohols. II. Acidities of Some Substituted Methanols and Related Compounds1, 2.* Journal of the American Chemical Society, 1960. **82**(4): p. 795-798.

30. Spange, S., T. Heinze, and D. Klemm, *On the polarity and donor-acceptor-properties of polysaccharides.* Polymer Bulletin, 1992. **28**(6): p. 697-702.

31. Kosan, B., K. Schwikal, and F. Meister, *Solution states of cellulose in selected direct dissolution agents.* Cellulose, 2010. **17**(3): p. 495-506.

32. Boerstoel, H., *Liquid Crystalline Solutions of Cellulose in Phosphoric Acid: For Preparing Cellulose Yarns*. 1998: University Library Groningen][Host].

33. Kroon-Batenburg, L.M.J., et al., *Estimation of the Persistence Length of Polymers by MD Simulations on Small Fragments in Solution. Application to Cellulose.* The Journal of Physical Chemistry B, 1997. **101**(42): p. 8454-8459.

34. Rein, D.M., et al., *True molecular solutions of natural cellulose in the binary ionic liquid-containing solvent mixtures.* Carbohydrate Polymers, 2014. **112**: p. 125-133.

35. Radhi, A., et al., *Macroscopic and microscopic study of 1-ethyl-3-methyl-imidazolium acetate-DMSO mixtures.* The Journal of Physical Chemistry B, 2015. **119**(4): p. 1633-1640.

36. Martin, D., A. Weise, and H.-J. Niclas, *The solvent dimethyl sulfoxide.* Angewandte Chemie International Edition, 1967. **6**(4): p. 318-334.

37. Hall, C.A., et al., *Macroscopic and microscopic study of 1-ethyl-3-methyl-imidazolium acetate-water mixtures.* The Journal of Physical Chemistry B, 2012. **116**(42): p. 12810-12818.

38. Partington, J.R., R.F. Hudson, and K.W. Bagnall, *Self-diffusion of aliphatic alcohols.* Nature, 1952. **169**(4301): p. 583-584.

39. Montalbán, M., et al., *Experimental measurements of octanol-water partition coefficients of ionic liquids.* J. Adv. Chem. Eng, 2015. **5**: p. 1000133.

40. Oliferenko, A.A., et al., *Theoretical scales of hydrogen bond acidity and basicity for application in QSAR/QSPR studies and drug design. Partitioning of aliphatic compounds.* Journal of chemical information and computer sciences, 2004. **44**(3): p. 1042-1055.

41. Mazzobre, M.F., et al., *Octanol-water partition coefficient of glucose, sucrose, and trehalose.* Carbohydrate research, 2005. **340**(6): p. 1207-1211.

42. Laurence, C. and M. Berthelot, *Observations on the strength of hydrogen bonding.* Perspectives in Drug Discovery and Design, 2000. **18**(1): p. 39-60.

43. Abraham, M.H., et al., *Hydrogen bonding. 32. An analysis of water-octanol and water-alkane partitioning and the ΔlogP parameter of Seiler.* Journal of pharmaceutical sciences, 1994. **83**(8): p. 1085-1100.

44. Izgorodina, E.I. and D.R. MacFarlane, *Nature of Hydrogen Bonding in Charged Hydrogen-Bonded Complexes and Imidazolium-Based Ionic Liquids.* The Journal of Physical Chemistry B, 2011. **115**(49): p. 14659-14667.

45. Endo, T., T. Kato, and K. Nishikawa, *Effects of Methylation at the 2 Position of the Cation Ring on Phase Behaviors and Conformational Structures of Imidazolium-Based Ionic Liquids.* The Journal of Physical Chemistry B, 2010. **114**(28): p. 9201-9208.

46. Fukaya, Y. and H. Ohno, *Hydrophobic and polar ionic liquids.* Physical Chemistry Chemical Physics, 2013. **15**(11): p. 4066-4072.

47. Parviainen, H., et al., *Dissolution enthalpies of cellulose in ionic liquids.* Carbohydrate Polymers, 2014. **113**: p. 67-76.

48. Le, K.A., C. Rudaz, and T. Budtova, *Phase diagram, solubility limit and hydrodynamic properties of cellulose in binary solvents with ionic liquid.* Carbohydrate polymers, 2014. **105**: p. 237-243.

49. Olmstead, W.N., Z. Margolin, and F.G. Bordwell, *Acidities of water and simple alcohols in dimethyl sulfoxide solution.* The Journal of organic chemistry, 1980. **45**(16): p. 3295-3299.

50. Hine, J. and M. Hine, *The Relative Acidity of Water, Methanol and Other Weak Acids in Isopropyl Alcohol Solution1*. Journal of the American Chemical Society, 1952. **74**(21): p. 5266-5271.

51. Scheiner, S., *Hydrogen bonding: a theoretical perspective*. 1997: Oxford University Press on Demand.

52. Olsson, C., et al., *Effect of methylimidazole on cellulose/ionic liquid solutions and regenerated material therefrom.* Journal of Materials Science, 2014. **49**(9): p. 3423-3433.

53. Liu, H., et al., *Understanding the interactions of cellulose with ionic liquids: a molecular dynamics study.* The Journal of Physical Chemistry B, 2010. **114**(12): p. 4293-4301.

54. Remsing, R.C., et al., *Solvation of carbohydrates in N, N'-dialkylimidazolium ionic liquids: A multinuclear NMR spectroscopy study.* The Journal of Physical Chemistry B, 2008. **112**(35): p. 11071-11078.

55. Stark, A., et al., *The effect of hydrogen bond acceptor properties of ionic liquids on their cellulose solubility.* Science China Chemistry, 2012: p. 1-8.

56. Shi, W., et al., *Theoretical and experimental studies of water interaction in acetate based ionic liquids.* Physical Chemistry Chemical Physics, 2012. **14**(45): p. 15897-15908.

57. de Oliveira, H.F.N. and R. Rinaldi, *Understanding cellulose dissolution: energetics of interactions of ionic liquids and cellobiose revealed by solution microcalorimetry.* ChemSusChem, 2015. **8**(9): p. 1577-1584.

58. Verma, V.K. and T. Banerjee, *Ionic liquids as entrainers for water+ethanol, water+2-propanol, and water+THF systems: A quantum chemical approach.* The Journal of Chemical Thermodynamics, 2010. **42**(7): p. 909-919.

59. Catalan, J., C. Diaz, and F. Garcia-Blanco, *Characterization of binary solvent mixtures of DMSO with water and other cosolvents.* The Journal of organic chemistry, 2001. **66**(17): p. 5846-5852.

60. Voronova, M., D. Batov, and A. Zakharov, *Sorption of water by cellulose from binary water-organic solutions.* Russian Journal of Physical Chemistry A, 2013. **87**(1): p. 104-107.

61. Bengtsson, J., et al., *Understanding the Inhibiting Effect of Small-Molecule Hydrogen Bond Donors on the Solubility of Cellulose in Tetrabutylammonium Acetate/DMSO.* The Journal of Physical Chemistry B, 2017. **121**(50): p. 11241-11248.

62. GalvaÌƒo, A.C., et al., *Sucrose Solubility in Binary Liquid Mixtures Formed by Waterâ€“Methanol, Waterâ€“Ethanol, and Methanolâ€“Ethanol at 303 and 313 K.* Journal of Chemical & Engineering Data. **61**(9): p. 2997-3002.

63. Radugin, M., et al., *Heat of dissolution of cellulose in water and water-dimethyl sulfoxide mixtures.* Fibre chemistry, 2008. **40**(6): p. 533-536.

64. Olsson, C., et al., *Influence of water on swelling and dissolution of cellulose in 1-ethyl-3-methylimidazolium acetate.* Carbohydrate polymers, 2014. **99**: p. 438-446.

65. Mazza, M., et al., *Influence of water on the dissolution of cellulose in selected ionic liquids.* Cellulose, 2009. **16**(2): p. 207-215.

66. Hauru, L.K., et al., *Role of solvent parameters in the regeneration of cellulose from ionic liquid solutions.* Biomacromolecules, 2012. **13**(9): p. 2896-2905.

67. Budtova, T. and P. Navard, *Cellulose in NaOH-water based solvents: a review.* Cellulose, 2016. **23**(1): p. 5-55.

68. Liu, R. and X. Hu, *Precipitation kinetics of cellulose in the Lyocell spinning process.* Industrial & engineering chemistry research, 2006. **45**(8): p. 2840-2844.

69. Gavillon, R. and T. Budtova, *Kinetics of cellulose regeneration from cellulose-NaOH-water gels and comparison with cellulose-N-methylmorpholine-N-oxide-water solutions.* Biomacromolecules, 2007. **8**(2): p. 424-432.

70. Biganska, O. and P. Navard, *Kinetics of precipitation of cellulose from cellulose-NMMO-water solutions.* Biomacromolecules, 2005. **6**(4): p. 1948-1953.

71. Hauru, L.K., et al., *Cellulose regeneration and spinnability from ionic liquids.* Soft matter, 2016. **12**(5): p. 1487-1495.

72. Jiang, G., et al., *Diffusion dynamics of 1-Butyl-3-methylimidazolium chloride from cellulose filament during coagulation process.* Cellulose, 2011. **18**(4): p. 921-928.

73. Sescousse, R., R. Gavillon, and T. Budtova, *Aerocellulose from cellulose-ionic liquid solutions: preparation, properties and comparison with cellulose-NaOH and cellulose-NMMO routes.* Carbohydrate polymers, 2011. **83**(4): p. 1766-1774.

74. Sescousse, R. and T. Budtova, *Influence of processing parameters on regeneration kinetics and morphology of porous cellulose from cellulose-NaOH-water solutions.* Cellulose, 2009. **16**(3): p. 417-426.

75. Laity, P., P. Glover, and J. Hay, *Composition and phase changes observed by magnetic resonance imaging during non-solvent induced coagulation of cellulose.* Polymer, 2002. **43**(22): p. 5827-5837.

76. Hedlund, A., T. Köhnke, and H. Theliander, *Coagulation of EmimAc-cellulose solutions: dissolution-precipitation disparity and effects of non-solvents and cosolvent.* NORDIC PULP & PAPER RESEARCH JOURNAL, 2015. **30**(1): p. 32-42.

77. Gericke, M., et al., *Rheological properties of cellulose/ionic liquid solutions: from dilute to concentrated states.* Biomacromolecules, 2009. **10**(5): p. 1188-1194.

78. Sescousse, R., et al., *Viscosity of cellulose-imidazolium-based ionic liquid solutions.* The Journal of Physical Chemistry B, 2010. **114**(21): p. 7222-7228.

79. Packer, K. and D. Tomlinson, *Nuclear spin relaxation and self-diffusion in the binary system, dimethylsulphoxide (DMSO)+ water.* Transactions of the Faraday Society, 1971. **67**: p. 1302-1314.

80. Gillen, K.T., D.C. Douglass, and M.J.R. Hoch, *Self-Diffusion in Liquid Water to -31° C.* The Journal of Chemical Physics, 1972. **57**(12): p. 5117-5119.

81. Meckl, S. and M. Zeidler, *Self-diffusion measurements of ethanol and propanol.* Molecular Physics, 1988. **63**(1): p. 85-95.

82. Hurle, R.L., A.J. Easteal, and L.A. Woolf, *Self-diffusion in monohydric alcohols under pressure. Methanol, methan (2 H) ol and ethanol.* Journal of the Chemical Society, Faraday Transactions 1: Physical Chemistry in Condensed Phases, 1985. **81**(3): p. 769-779.

83. Wang, S., A. Lu, and L. Zhang, *Recent advances in regenerated cellulose materials.* Progress in Polymer Science, 2016. **53**: p. 169-206.

84. Kosan, B., C. Michels, and F. Meister, *Dissolution and forming of cellulose with ionic liquids.* Cellulose, 2008. **15**(1): p. 59-66.

85. Michud, A., M. Hummel, and H. Sixta, *Influence of molar mass distribution on the final properties of fibers regenerated from cellulose dissolved in ionic liquid by dry-jet wet spinning.* Polymer, 2015. **75**: p. 1-9.

86. Michud, A., et al., *Ioncell-F: ionic liquid-based cellulosic textile fibers as an alternative to viscose and Lyocell.* Textile Research Journal, 2016. **86**(5): p. 543-552.

87. Olsson, C. and G. Westman, *Wet spinning of cellulose from ionic liquid solutions: viscometry and mechanical performance.* Journal of Applied Polymer Science, 2013. **127**(6): p. 4542-4548.